Bionanotech - proteins

- Engineering
- Design
- Catalysis
- Self-assemblies
- Templates & scaffolds
- Surface coatings
- Sensors

Tuan Vo-Dinh, Fitzpatrick Institute for Photonics

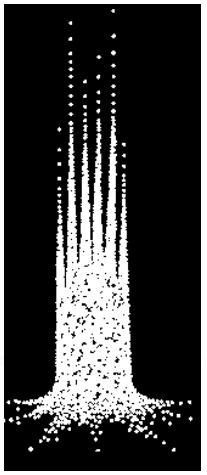

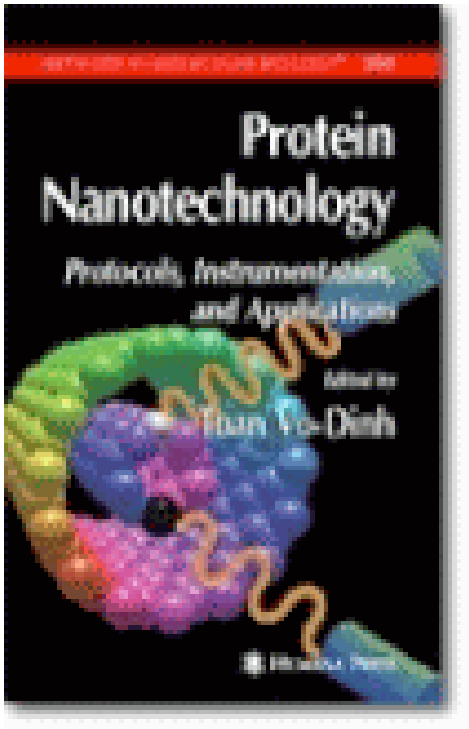

Humana Press

- Nanostructures and self-assemblies
- Drug delivery
- Biosensors
- Molecularly imprinted polymers

Protein Nanotech

- Engineered assemblies
- Organization of nanomaterials
- Biosensors
- Biomineralization

Biological Species	Example	Typical size	MW (daltons)
Small protein	Chymotrypsin	4 nm sphere	10^4-10^5
Large protein	Asp.transcarb.	7 nm sphere	10^5-10^7
Small assembly	Ribosome	20 nm sphere	10^5-10^7
Large assembly	Viruses	100 nm sphere	10^7-10^{12}
Nucleic acids	tRNA	10 nm rod	10^4-10^5

Nanohedra: Using symmetry to design self assembling protein cages, layers, crystals, and filaments

Jennifer E. Padilla*†‡, Christos Colovos*†‡, and Todd O. Yeates*‡§

*Department of Chemistry and Biochemistry, and ‡Department of Energy Laboratory of Structural Biology and Molecular Medicine, University of California, Los Angeles, CA 90095-1569

PNAS | February 27, 2001 | vol. 98 | no. 5 | 2217–2221

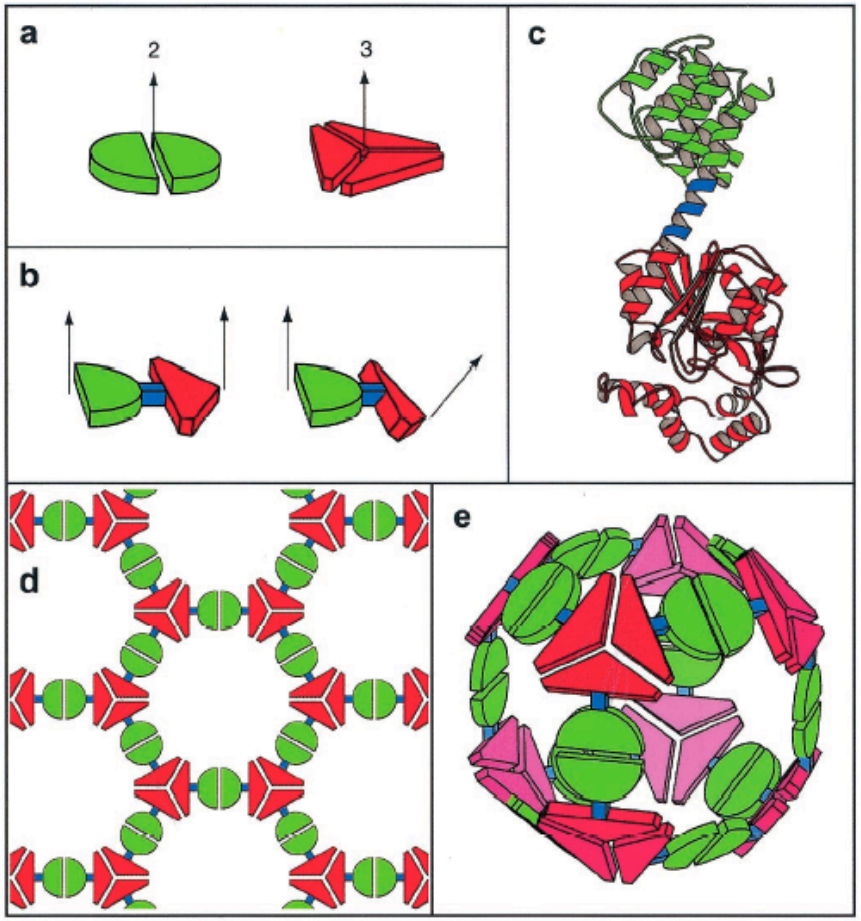

Fig. 1. A general strategy for designing fusion proteins that assemble into symmetric nanostructures. (*a*) The green semicircle represents a natural dimeric protein (i.e., a protein that associates with one other copy of itself), whereas the red shape represents a trimeric protein. The symmetry axes of the natural oligomers are shown. (*b*) The two natural proteins are combined by genetic methods into a single fusion protein. Each of the original natural proteins serves as an "oligomerization domain" in the designed fusion protein. Two different hypothetical fusion proteins are shown to illustrate that the oligomerization domains can be joined rigidly in different geometries. (*c*) A ribbon diagram of a fusion protein showing one method for joining two oligomerization domains (red and green) in a relatively rigid fashion. One of the natural oligomerization domains must end in an α-helical conformation, and the other must begin in an α-helical conformation. The two are then linked by a short stretch of amino acids (blue) that have a strong tendency to adopt an α-helical conformation. Thus, the two oligomerization domains are joined physically in a predictable orientation. (*d*) A designed fusion protein self assembles into a particular kind of nanostructure that depends on the geometry of the symmetry axes belonging to its component oligomerization domains (Table 1). A molecular layer arises from an arrangement like that in *b* (*Left*). (*e*) A cubic cage arises from an arrangement like the one in *b* (*Right*).

PNAS | February 27, 2001 | vol. 98 | no. 5 | 2217–2221

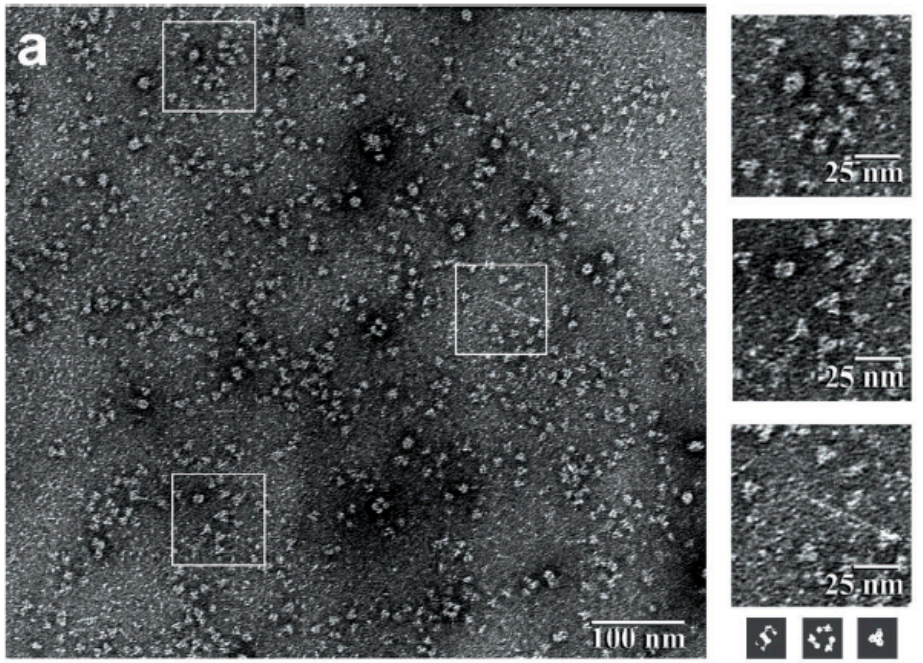

Table 1. Construction rules for designing nanohedral protein materials from dimeric and trimeric oligomerization domains

Symmetry*	Construction	Geometry of symmetry elements†	
Cages and shells			
T‡	Dimer-trimer	54.7°	I
O§	Dimer-trimer	35.3°	I
I	Dimer-trimer	20.9°	I
Double-layer rings			
D_n	Dimer-dimer	180°/*n*	I
Two-dimensional layers			
p6¶	Dimer-trimer	0°	N
p321	Dimer-trimer	90°	N
p3	Trimer-trimer	0°	N
Three-dimensional crystals			
$I2_13$	Dimer-trimer	54.7°	N
$P4_132$ or $P4_332$	Dimer-trimer	35.3°	N
P23	Trimer-trimer	70.5°	N
Helical filaments			
Helical‖	Dimer-dimer	Any angle,	N

This table gives only those symmetries that can be constructed by combining two oligomerization domains of the dimeric or trimeric type. Other kinds of oligomerization domains, such as tetramers, would give additional possibilities not listed here.

*T, O, I, and D_n refer to tetrahedral, octahedral, icosahedral, and dihedral symmetry, respectively. The remaining symbols are denoted by their Hermann–Mauguin symbols.

†The angle formed between the two symmetry elements is given, followed by I or N to denote intersecting or nonintersecting axes.

PNAS | February 27, 2001 | vol. 98 | no. 5 | 2217–2221

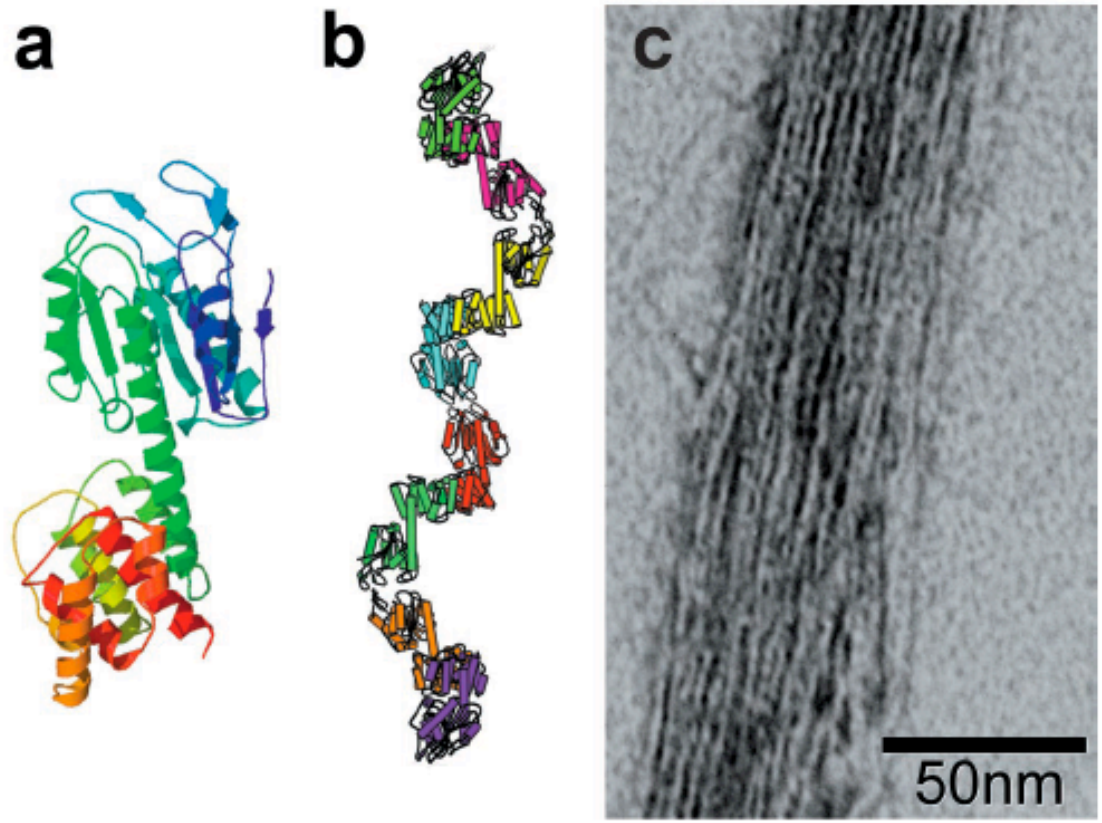

Fig. 3. Electron microscopy and model of a designed protein filament. (*a*) A ribbon model of a single molecule of the designed fusion protein. (*b*) A ribbon model of the protein filament as it was intended to assemble, with separate protein molecules colored differently. (*c*) Negatively stained electron micrograph of a bundle of filaments formed by the designed fusion protein. The bundle is 15–20 filaments across and reveals details indicative of the individual dimeric oligomerization domains that make up the fusion protein. In addition to bundles, networks of filaments were also observed in other micrographs.

Self-Assembly of Proteins into Designed Networks

Philippe Ringler and Georg E. Schulz*

3 OCTOBER 2003 VOL 302 SCIENCE

A C_4-symmetric tetrameric aldolase was used to produce a quadratic network consisting of the enzyme as a rigid four-way connector and stiff streptavidin rods as spacers. Each aldolase subunit was furnished with a His_6 tag for oriented binding to a planar surface and two tethered biotins for binding streptavidin in an oriented manner. The networks were improved by starting with composite units and also by binding to nickel–nitrilotriacetic acid–lipid monolayers. The mesh was adjustable in 5-nanometer increments. The production of a net with switchable mesh was initiated with the use of a calcium ion–containing β-helix spacer that denatured on calcium ion depletion.

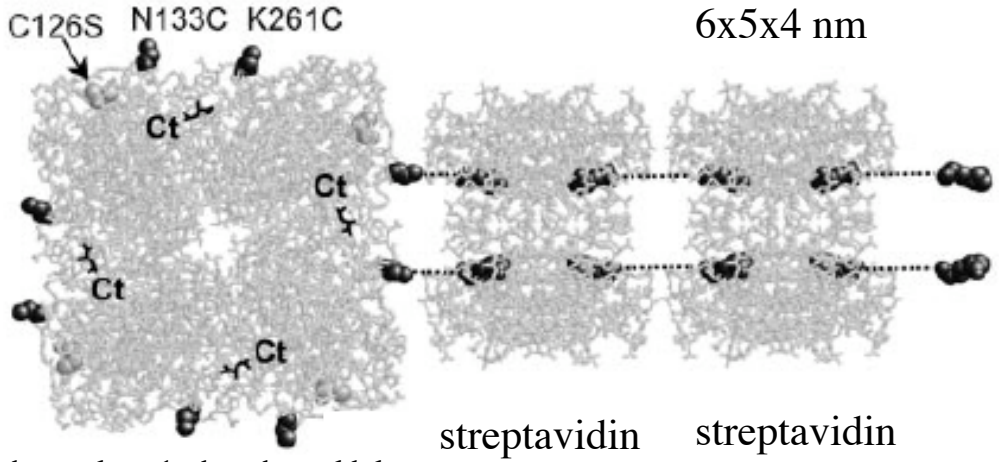

Protein arrays

3 OCTOBER 2003 VOL 302 SCIENCE

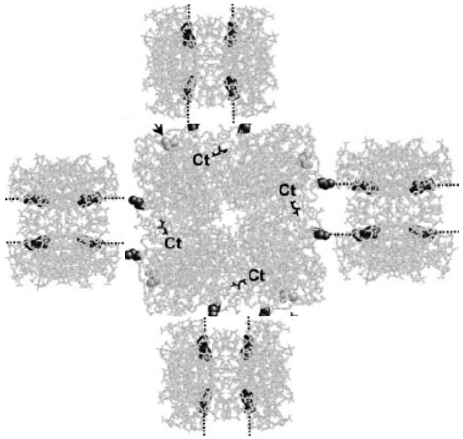

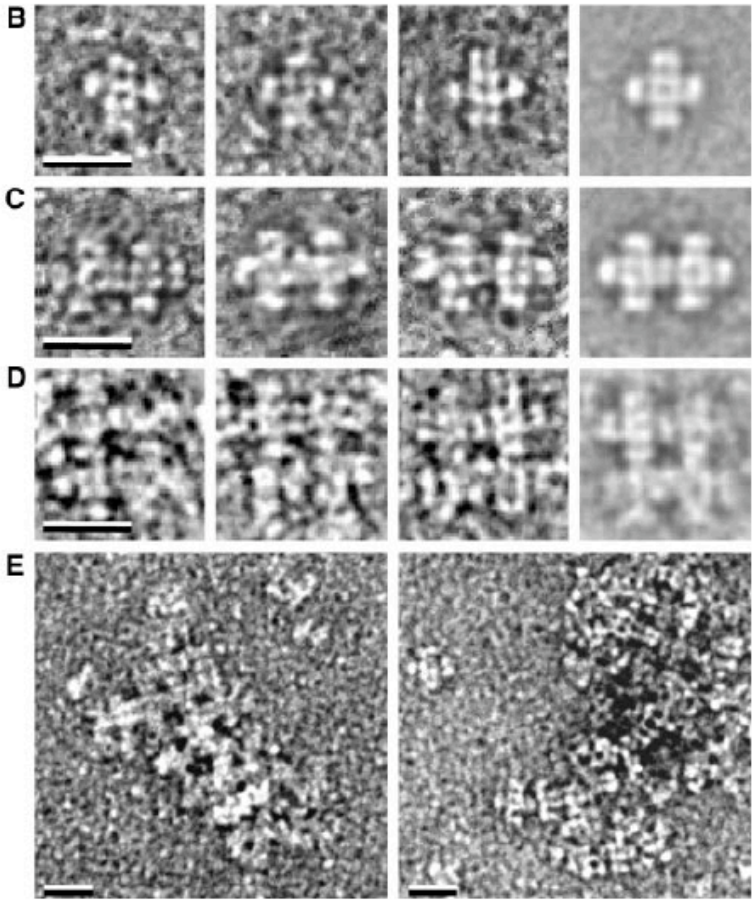

Fig. 1. Block construction and self-assembly in solution. All electron micrographs were negatively stained; all scale bars are 20 nm. The particles and nets were picked from numerous similar pictures. (**A**) View onto the flat 7-nm-by-7-nm top face (depth of 6 nm) of the C_4-symmetric enzyme RhuA (*14*). The point mutations for biotin labeling are stated for one subunit. The C termini (Ct) at the top face carry His_6 tags (*18*). Block ^{b}R is RhuA with eight tethered (dashed lines) biotins at the newly introduced cysteines, two of which are depicted as binding to a streptavidin (block S). The 6-nm-by-5-nm face (depth of 4 nm) of S is shown (*15*, *16*). The $^{b}R{\cdot}S$ unit is in turn bound to block ^{bb}S, which is a streptavidin with (the four depicted) bis-biotin linkers. (**B**) Block $^{b}R{\cdot}S_4$ produced on a Ni-NTA column (*18*). Three samples and an average of 21 are given. (**C**) Block $^{b}R_2{\cdot}S_7$, which occasionally eluted from the Ni-NTA column, showing three samples and an average of 11. (**D**) Block $^{b}R_4S_{12}$ produced as a by-product during self-assembly of ^{b}R and $^{b}R{\cdot}S_4$. Three samples and an average of six are shown. The shortest distances between ^{b}R units are around 13 nm, confirming the presence of one S as spacer. (**E**) Networks produced by self-assembly of ^{b}R and $^{b}R{\cdot}S_4$, reaching sizes of 50 nm by 50 nm.

Protein arrays

3 OCTOBER 2003 VOL 302 SCIENCE

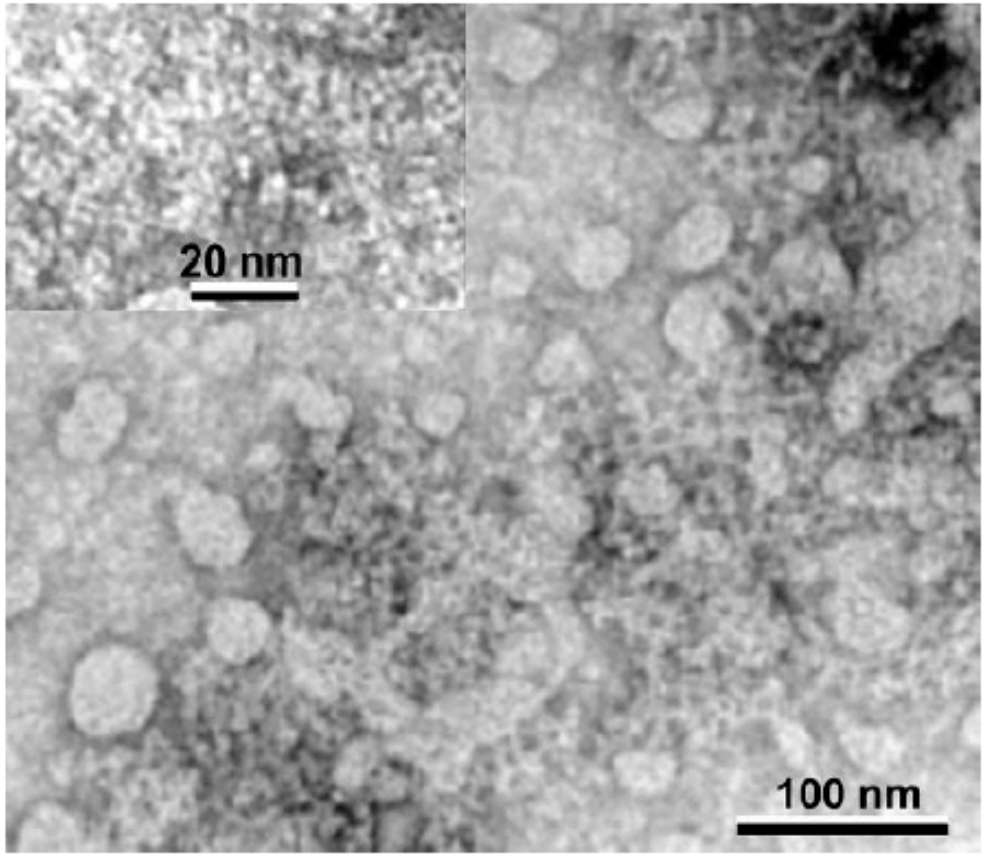

Fig. 2. Representative negatively stained example of the networks formed by self-assembly of blocks ^{b}R and $^{b}R{\cdot}S_4$ at a lipid monolayer. The lattices extend over more than 200 nm by 200 nm but contain irregularities. (**Insert**) A magnified sample.

Protein arrays

3 OCTOBER 2003 VOL 302 SCIENCE

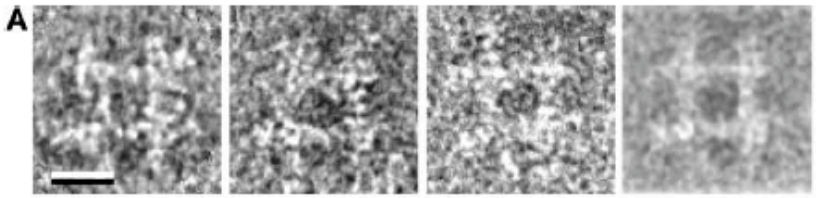

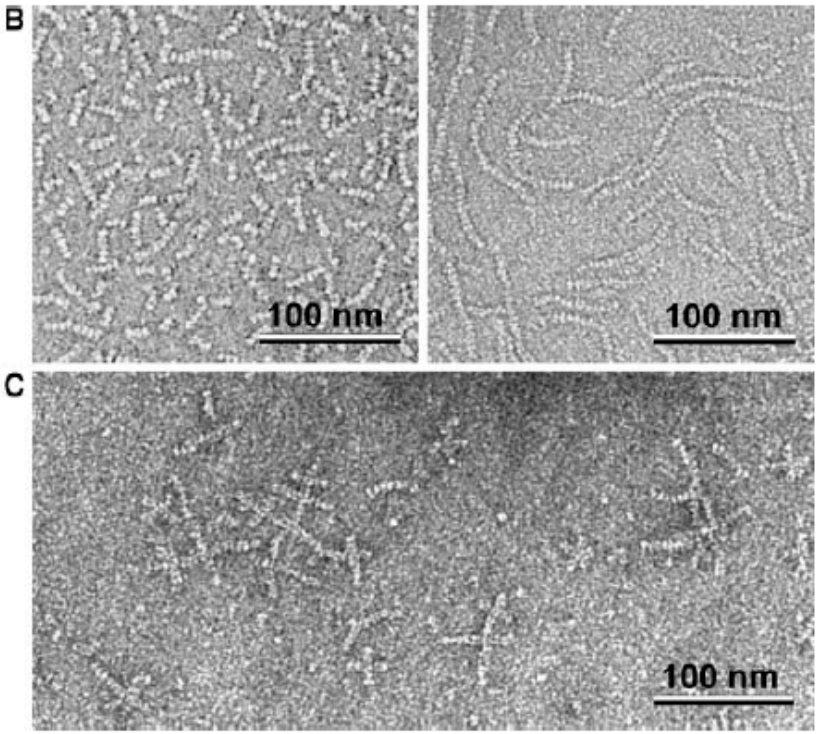

Fig. 3. Networks with streptavidin spacer rods produced in solution. The electron micrographs are negatively stained. The depicted samples are representative. (**A**) Block $^{b}R_4{\cdot}S_{16}{\cdot}^{bb}S_{12}$ produced by self-assembly of $^{b}R{\cdot}S_4$ with ^{bb}S, showing three samples and an average of six. The distance between ^{b}R blocks is 21 nm (scale bar, 20 nm), in agreement with the expected $S{\cdot}^{bb}S{\cdot}S$ spacer. (**B**) Streptavidin rods of around five units produced by mixing ^{bb}S with a smaller amount of S (left). Longer rods of around 20 units obtained by mixing equal particle numbers of the five-unit rods and S (right). (**C**) Self-assembly of $^{b}R{\cdot}S_4$ with $(^{bb}S{\cdot}S)_x$ ^{bb}S rods (*18*) of various lengths.

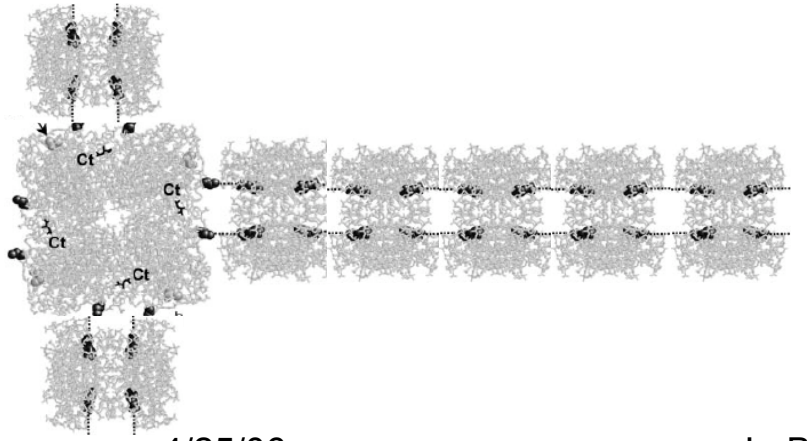

Protein arrays

3 OCTOBER 2003 VOL 302 SCIENCE

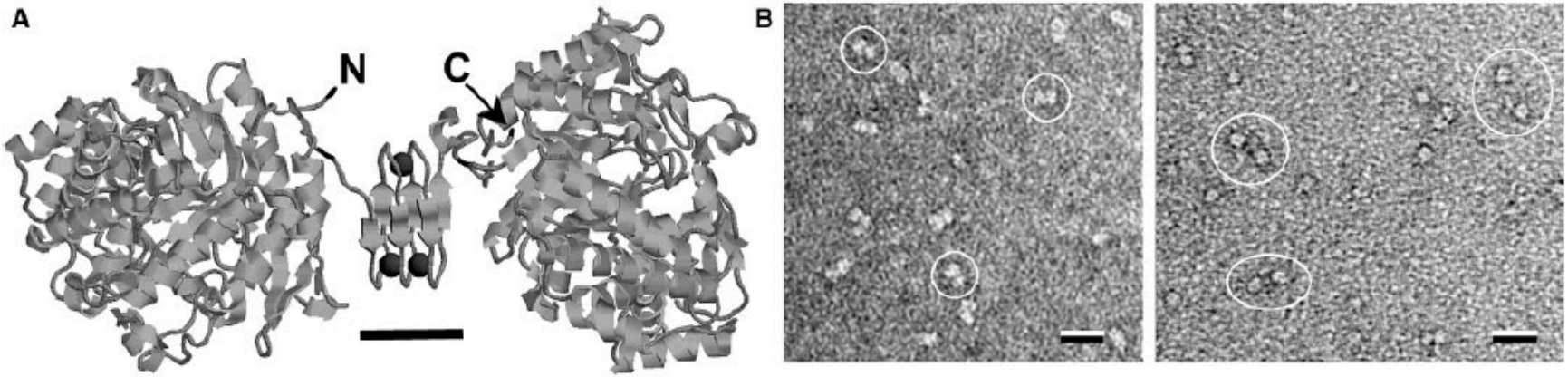

Fig. 4. The 998-residue construct PGAL-β-PGAL (*17*, *18*). (**A**) Ribbon model of the polypeptide indicating N and C termini of the construct. On Ca^{2+} removal, the β helix (scale bar, 2 nm) denatures, giving rise to a 20-nm peptide tether. (**B**) Electron micrographs of negatively stained solutions of PGAL-β-PGAL picked from numerous similar pictures (scale bars, 20 nm). The left side shows PGAL-β-PGAL after EDTA-free preparation (*22*), forming dumbbell-shaped particles (circled) corresponding to the model of (A). On the right side, the same preparation after treatment with 10 mM EDTA shows separated globular PGAL molecules (the denatured peptide is not visible).

Protein arrays

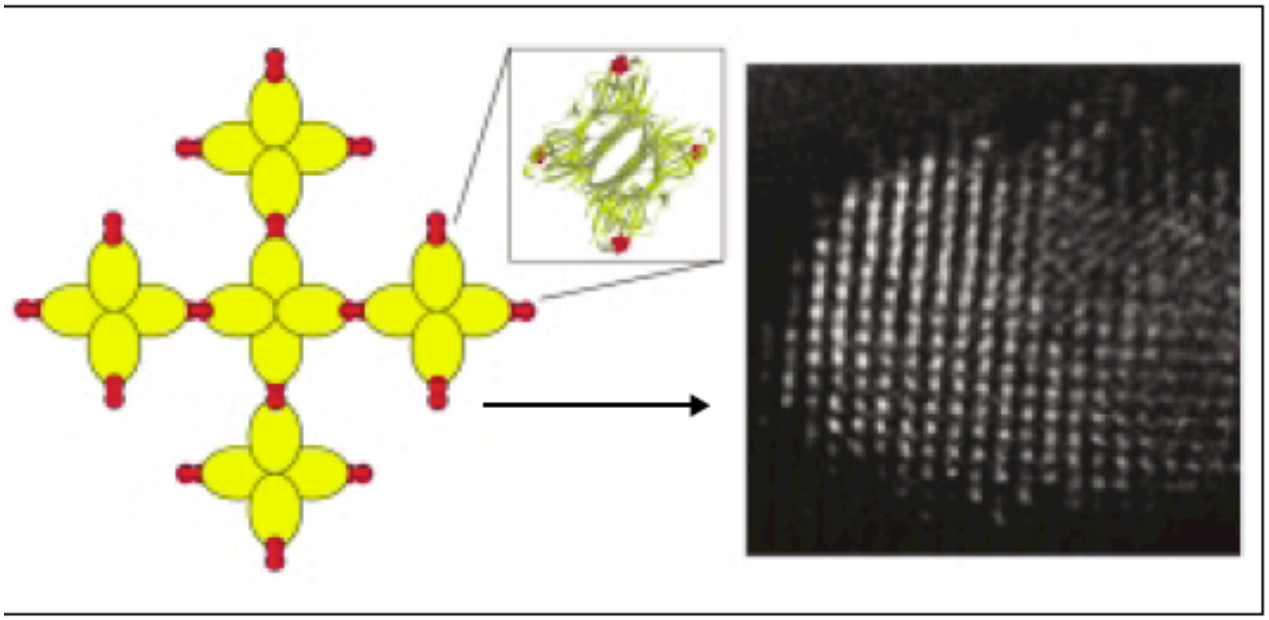

A strategy for creating regular protein arrays from a natural oligomeric protein and a bivalent ligand [42]. In the case illustrated, a tetrameric lectin (four yellow ellipses) was mixed with a synthetic, two-headed carbohydrate molecule (red). Each protein complex is polyvalent by virtue of its ability to contact four other complexes. The result was an ordered three-dimensional material with subunits arranged in a 'diamond-like' lattice. A ribbon model of the tetrameric protein is shown (in the inset), as is a transmission electron micrograph of the material. Dotan *et al.* measured 6.9 ± 0.3 nm between the centers of neighboring molecules in the micrograph. Reprinted with permission from [42], copyright 1999 Wiley-VCH.

42. Dotan N, Arad D, Frolow F, Freeman A: **Self-assembly of a tetrahedral lectin into predesigned diamond-like protein crystals.** *Angew Chem Int Ed Engl* 1999, **38**:2363-2366.

Bionanotech - proteins

- Engineering
- Design
- Catalysis
- Self-assemblies
- Templates & scaffolds
- Surface coatings
- Sensors

Ordered nanoparticle arrays formed on engineered chaperonin protein templates

R. ANDREW MCMILLAN*[1], CHAD D. PAAVOLA[1], JEANIE HOWARD[2], SUZANNE L. CHAN[2], NESTOR J. ZALUZEC[3] AND JONATHAN D. TRENT*[1]

[1]NASA Ames Research Center, Center for Nanotechnology and Astrobiology Technology Branch, Mail Stop 239-15, Moffett Field, California 94035, USA
[2]SETI Institute, 2035 Landings Drive, Mountain View, California 94043, USA
[3]Argonne National Laboratory, Materials Science Division, 9700 South Cass Avenue, Argonne, Illinois 60439, USA
*e-mail: amcmillan@mail.arc.nasa.gov; jtrent@mail.arc.nasa.gov

nature materials | VOL 1 | DECEMBER 2002

- Chaperonins
  - Natural function: protein folding assistants or actually misfolding “inhibitor”.
  - Heat-shock protein.
  - Multimer assembles given ATP & Mg^{++}; large internal cavity.
  - 15 - 20 nm assemblies.
- *Sulfolobus shibatae*
  - Lives in geothermal hot-springs (85°C, pH 2).
  - Theromstable protein easy to purify and engineer.
  - Sequence & structure available for modeling.
  - Assembles into higher order structures (2D crystals).

Ordered nanoparticle arrays formed on engineered chaperonin protein templates

R. ANDREW MCMILLAN*[1], CHAD D. PAAVOLA[1], JEANIE HOWARD[2], SUZANNE L. CHAN[2], NESTOR J. ZALUZEC[3] AND JONATHAN D. TRENT*[1]

[1]NASA Ames Research Center, Center for Nanotechnology and Astrobiology Technology Branch, Mail Stop 239-15, Moffett Field, California 94035, USA
[2]SETI Institute, 2035 Landings Drive, Mountain View, California 94043, USA
[3]Argonne National Laboratory, Materials Science Division, 9700 South Cass Avenue, Argonne, Illinois 60439, USA
*e-mail: amcmillan@mail.arc.nasa.gov; jtrent@mail.arc.nasa.gov

nature materials | VOL 1 | DECEMBER 2002

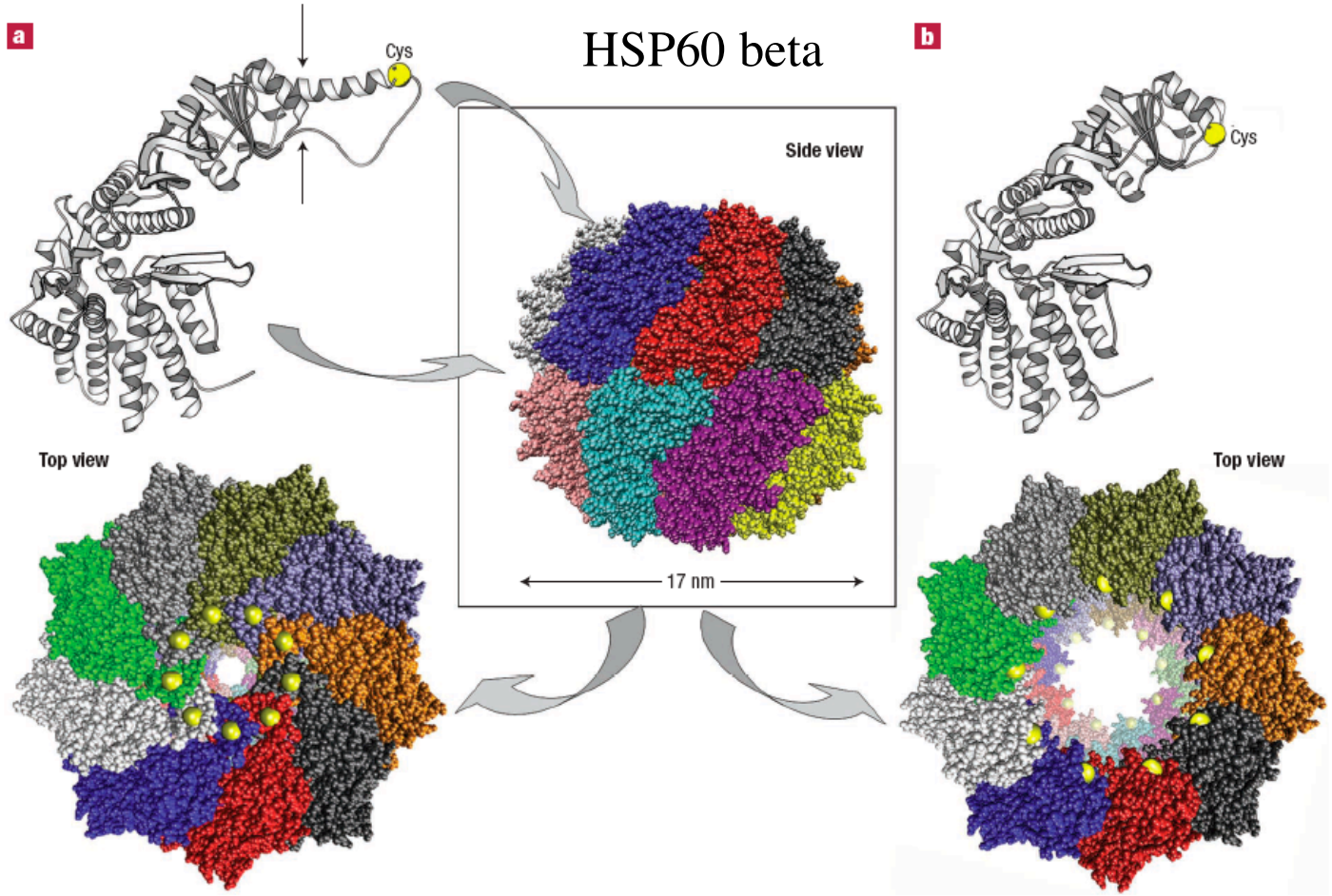

3 nm pore

9 nm pore

Chaperonin arrays

nature materials | VOL 1 | DECEMBER 2002

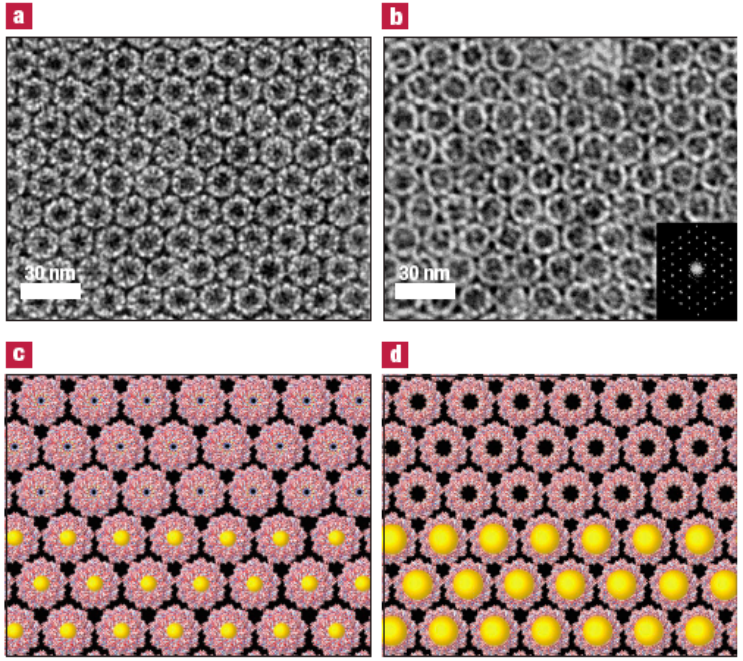

Figure 2 2D crystals of engineered chaperonins as quantum dot array templates. **a**, TEM image of a negatively stained 2D crystal of the beta chaperonin variant with cysteine substitutions at the apical pores. The two-sided-plane group p312 was assigned to the lattice through image analyses of micrographs of *S. shibatae* beta chaperonin 2D

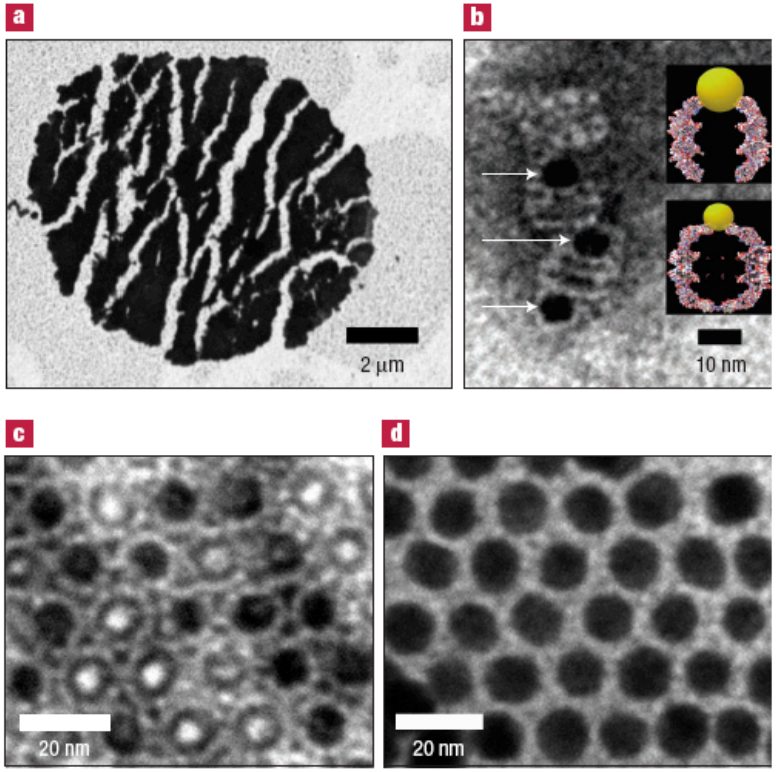

Figure 3 Gold QD binding to engineered chaperonins and chaperonin-templates. **a**, Low-magnification TEM image of 10 μm diameter 2D crystal of the 9-nm-pore chaperonin variant with bound 10 nm gold QDs. The image contrast is from gold QDs bound to the crystalline lattice of the underlying protein template. Drying causes significant sample cracking and contributes to distortions and separation of regions of order within the array. **b**, Higher-magnification stained TEM image of side views of 5 nm gold QDs (arrowed) tethered at the apical pores of the 3-nm-pore mutant chaperonins. Inset: Slab-view cutaway diagrams of postulated orientation of 5 and 10 nm gold QDs bound at the apical pores of the two chaperonin variants. **c**, Stained image of 5 nm gold QDs bound within the pores of the 3-nm-pore crystalline template. Occupied rings show the QDs (dark areas) are surrounded and held in place by the chaperonin pores. Empty rings have a brighter, less electron-dense appearance. We are currently investigating why some sites are unoccupied. We suspect that this is related to the solvent accessibility of thiols on the apical loops, or to the size variation of the 5 nm QDs. **d**, Ordered region of 10 nm gold bound to a 9-nm-pore template with similar area coverage as in **c**. The chaperonins are occluded by the 10 nm QDs.

Chaperonin arrays

nature materials | VOL 1 | DECEMBER 2002

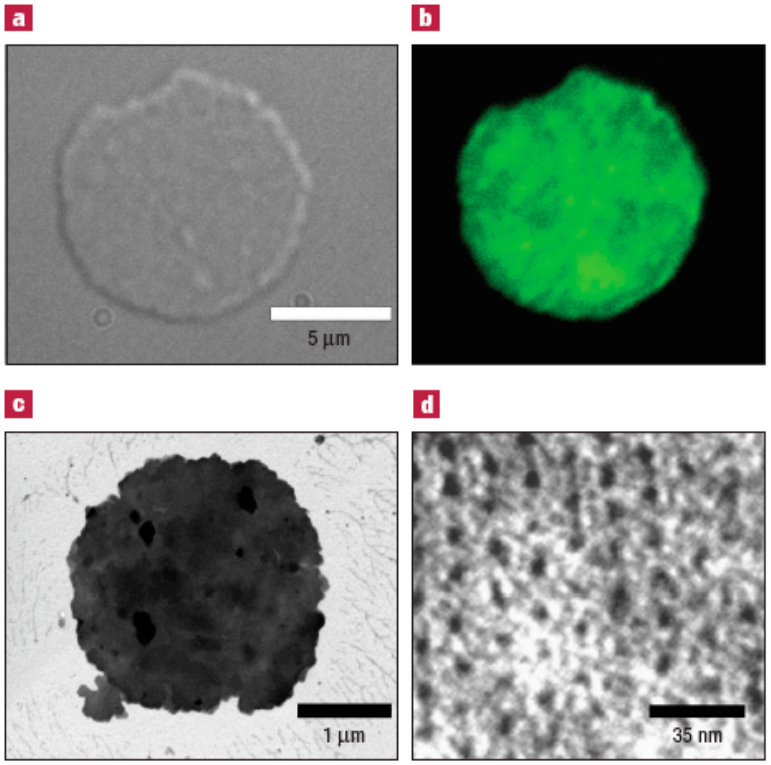

Figure 4 Semiconductor QD arrays. a, DIC light micrograph of an 8 µm crystalline disc of the 3-nm-pore template with bound 4.5 nm luminescent CdSe–ZnS QDs. **b**, Both dry and rehydrated arrays fluoresced indicating the QDs bound to the template. 2D crystals of a beta variant without added cysteines showed minimal QD binding (see Supplementary Information). **c**, Low-magnification TEM of an unstained array of CdSe–ZnS QDs. Image contrast is due to the bound semiconductor QDs. **d**, Higher-magnification image of the same crystal showing an ordered region of QDs bound to the chaperonin lattice.

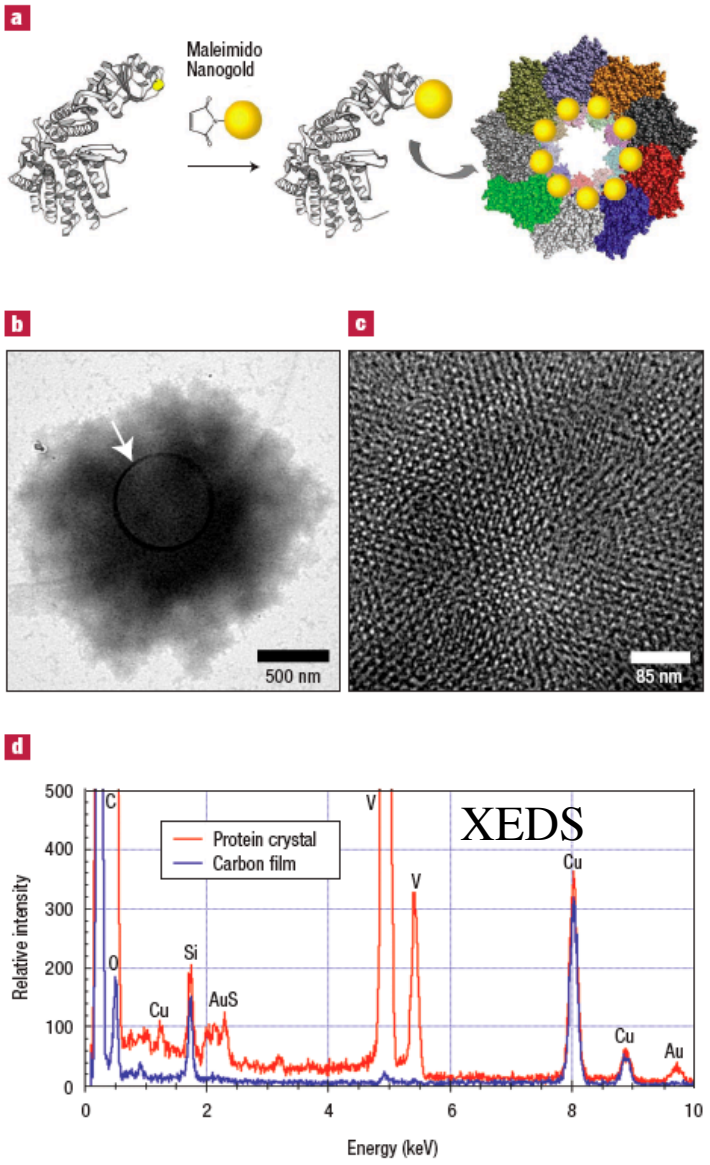

Figure 5 Chaperonin subunit mediated self-assembled Nanogold arrays. a, Covalent attachment of 1.4 nm monomaleimido Nanogold to subunits of the 9-nm-pore beta chaperonin variant through Michael addition of cysteine thiol to QD surface maleimide groups. Right: The possible arrangement of nine 1.4 nm covalently attached Nanogold QDs

S-layer arrays

bottom: *Methanocorpusculum sinense* DSM 4274 (magnification 343000 times)

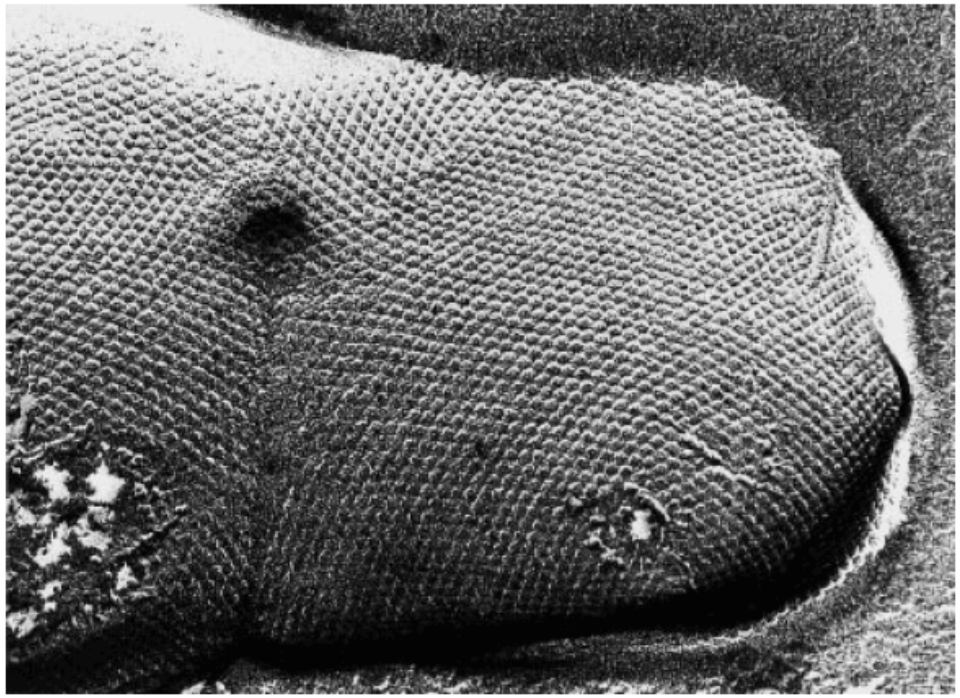

- Crystalline bacterial cell surface layers.
  - ~5x10^5 monomers/cell
  - Biosynth ~500 copies/sec
- Purified S-layer proteins self-assemble into arrays.
- Pores and functional groups available for engineering.

Crystalline Bacterial Cell Surface Layers (S Layers): From Supramolecular Cell Structure to Biomimetics and Nanotechnology

Uwe B. Sleytr,* Paul Messner, Dietmar Pum, and Margit Sára

Angew. Chem. Int. Ed. **1999**, *38*, 1034 – 1054

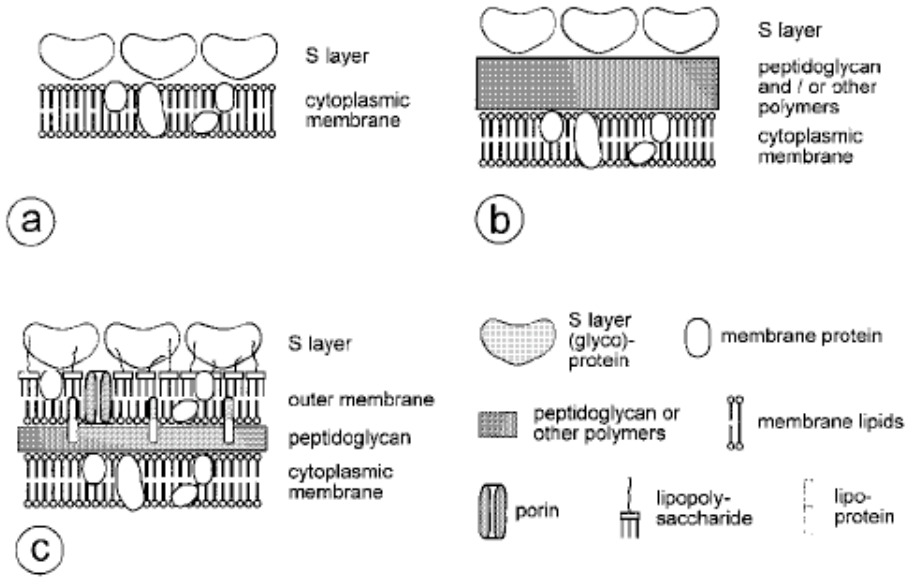

Figure 1. Schematic illustration of the supramolecular architecture of the three major classes of prokaryotic cell envelopes containing crystalline bacterial cell surface layers (S layers). a) Cell envelope structure of Gram-negative archaea with S layers as the only cell-wall component external to the cytoplasmic membrane. b) Cell envelope as observed in Gram-positive archaea and bacteria. In bacteria the rigid wall component is primarily composed of peptidoglycan. In archaea other wall polymers (e.g. pseudomurein or methanochondroitin) are found. c) Cell envelope profile of Gram-negative bacteria composed of a thin peptidoglycan layer and an outer membrane. If present the S layer is closely associated with the lipopolysaccharide of the outer membrane (modified based on reference [13]).

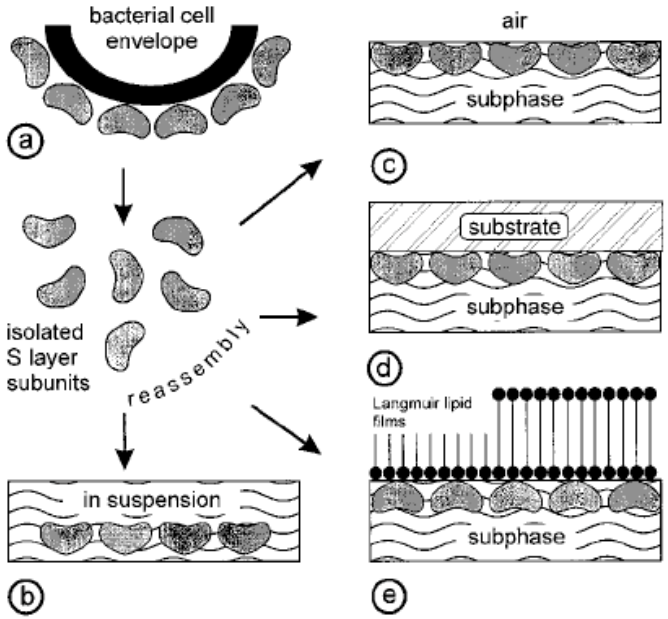

Figure 6. Schematic illustration of the recrystallization of isolated S layer subunits into crystalline arrays (a). The self-assembly process can occur in suspension (b), at the air/water interface (c), on solid supports (d), and on Langmuir lipid films (e).

S-layer arrays

Angew. Chem. Int. Ed. **1999**, *38*, 1034 – 1054

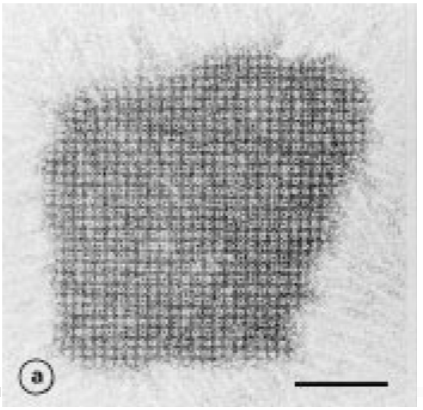

p4

p4 p6

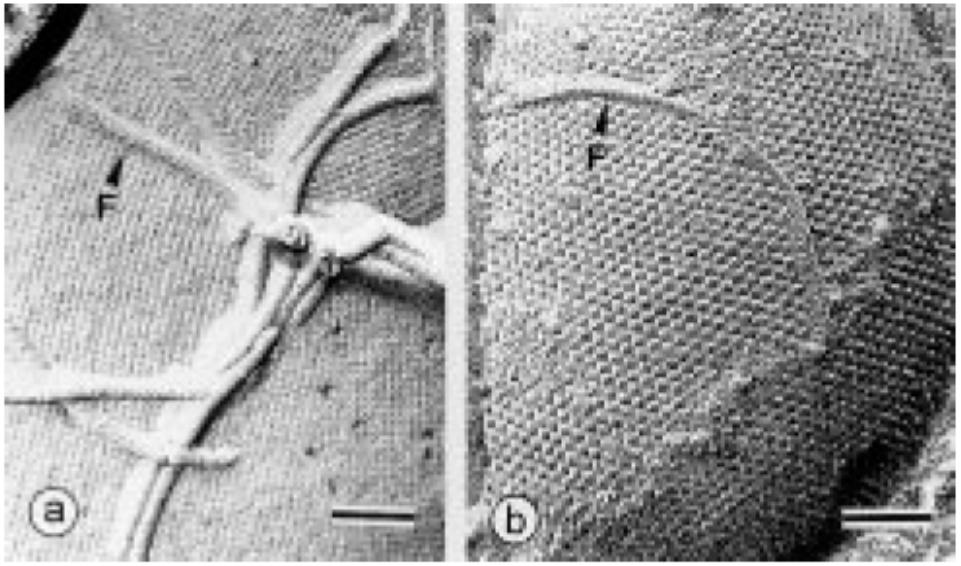

Figure 2. Electron micrograph of freeze-etched preparations of intact cells from a) *Aneurinibacillus thermoaerophilus* DSM 10155 showing a square (p4) S layer lattice and b) archaeon *Methanomicrobium mobile* DSM 1539 covered with a hexagonal (p6) array. F: flagella. The bar corresponds to 100 nm.

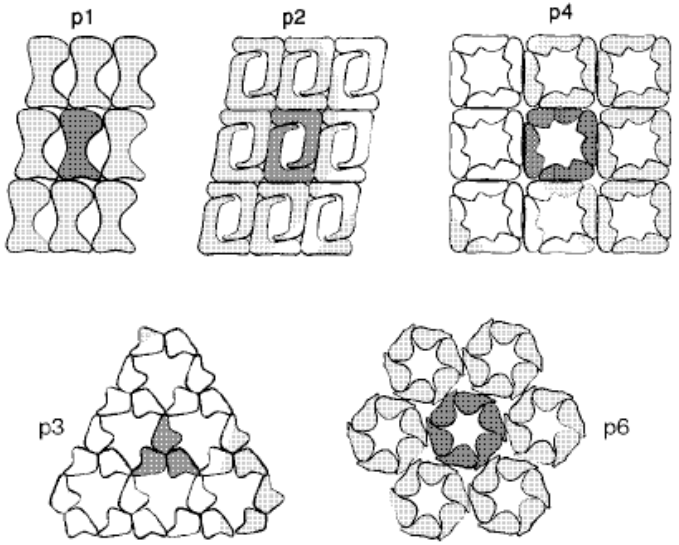

Figure 3. Schematic drawing of different S layer lattice types. The regular arrays exhibit either oblique (p1, p2), square (p4), or hexagonal lattice symmetry (p3, p6). The morphological units are composed of one, two, three, four, or six identical subunits.

S-layer arrays

Angew. Chem. Int. Ed. **1999**, *38*, 1034 – 1054

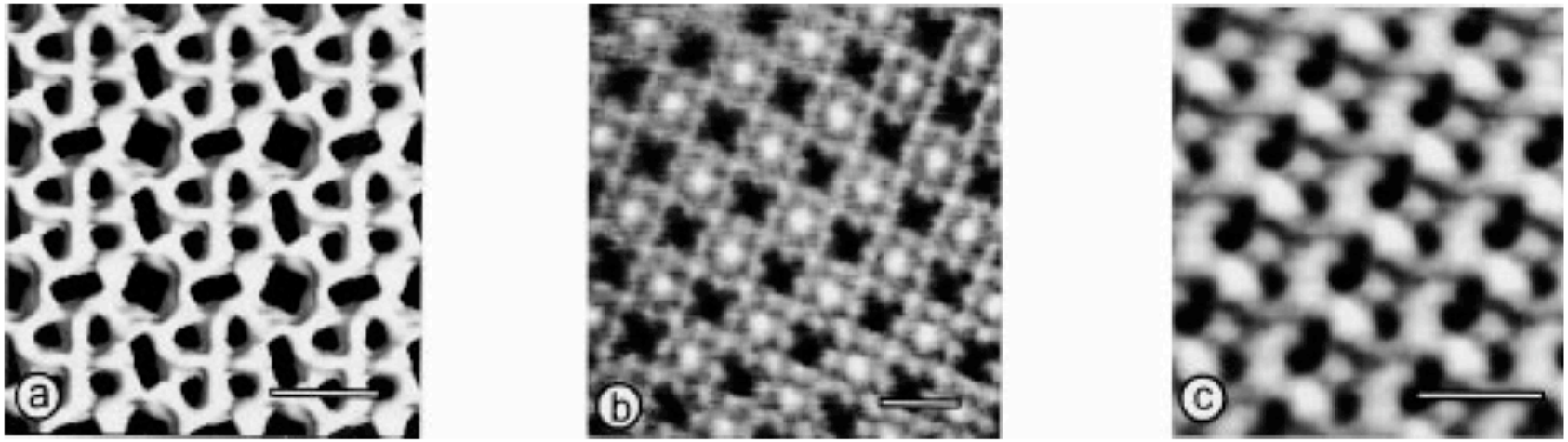

Figure 4. a) Three-dimensional model of the protein mass distribution of the S layer of *Bacillus stearothermophilus* NRS 2004/3a/V2 (outer face). The S layer is about 8 nm thick and exhibits a center-to-center spacing of the morphological units of 13.5 nm. The protein meshwork shows one square-shaped, two elongated, and four small pores per morphological unit. The model was obtained after recording several tilt series of a negatively stained preparation in a transmission electron microscope, performing Fourier-domain computer image reconstructions over each individual tilted view, and combining all processed views to a three-dimensional data volume. b), c) Computer image reconstruction of the scanning force microscopic images of the topography of the inner face of the S layer lattice from *B. sphaericus* CCM 2177 (b) and *Bacillus coagulans* E38 – 66/V1 (c). The images were taken under water. The surface corrugation corresponding to a gray scale from black to white is 1.8 nm. The center-to-center spacing of the morphological unit of the square lattice (b) is 14.5 nm. The S layer lattice in (c) shows an oblique unit cell ($a = 9.4$ nm, $b = 7.5$ nm, base angle $= 80°$). The bars correspond to 10 nm.

S-layer arrays

Angew. Chem. Int. Ed. **1999**, *38*, 1034 – 1054

Table 1. Properties of S layers.[5, 7, 14, 26, 43, 44, 54, 55]

The S layer lattices can have oblique (p1, p2), square (p4), or hexagonal (p3, p6) symmetry.
The center-to-center spacing of the morphological unit can be between 3 and 35 nm.
The lattices are generally 5 to 20 nm thick (in archaea up to approximately 70 nm).
The outer surface is generally less corrugated than the inner surface.
The S layer lattices exhibit pores of identical size and morphology.
In many S layers two or even more distinct classes of pores are present.
The pore sizes range from approximately 2 to 8 nm.
The pores can occupy 30 to 70 % of the surface area.
The relative molecular mass of constituent subunits is in the range of 40000 to 200000.
These are weakly acidic proteins (pI $\approx$ 4 – 6), except for *Methanothermus fervidus* (pI = 8.4) and lactobacilli (pI > 9.5).
Large amounts of glutamic and aspartic acid (about 15 mol %) are present.
There is a high lysine content (about 10 mol %).
There are large amounts of hydrophobic amino acids (about 40 – 60 mol %).
Hydrophilic and hydrophobic amino acids do not form extended clusters.
In most S layer proteins about 20 % of the amino acids are organized as α helices and about 40 % occur as β sheets.
Aperiodic foldings and β-turn content may vary between 5 and 45 %.
Posttranslational modifications of S layer proteins include cleavage of N- or C-terminal fragments, glycosylation, and phosphorylation of amino acid residues.

S-layer arrays

Angew. Chem. Int. Ed. **1999**, *38*, 1034 – 1054

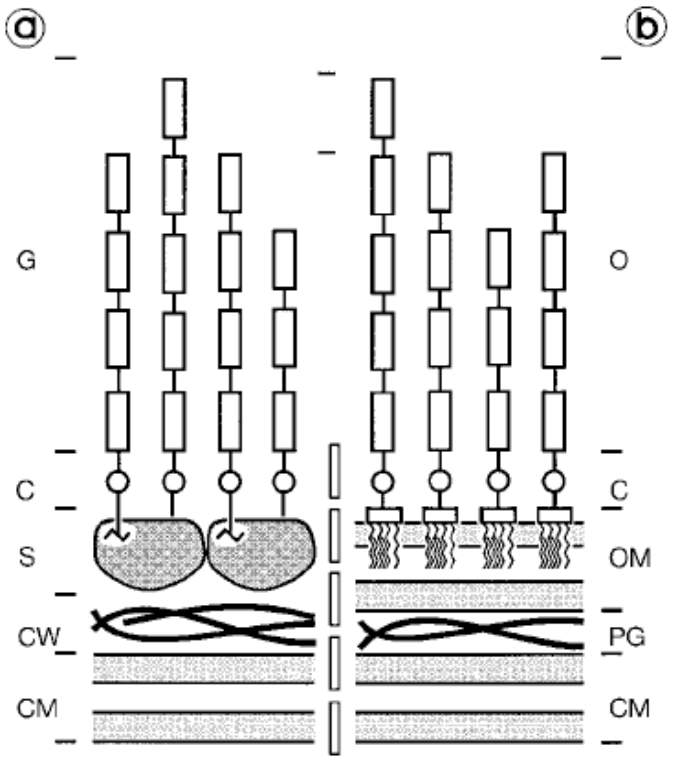

Figure 8. Schematic drawing of the cell envelope profile of Gram-positive (a) and Gram-negative bacteria (b) underlining the structural similarities between S layer glycoproteins and lipopolysaccharides. Abbrevations: C: core region; CM: cytoplasmic membrane; CW: cell wall; G: glycan chain; O: O-antigen; OM: outer membrane; PG: peptidoglycan (taken from reference [43] with permission of Landes/Academic Press).

- Diversity of:
  - Geometry
  - Pore size
  - pI
  - Glycosylation sites
  - Etc.

S-layer arrays

Angew. Chem. Int. Ed. **1999**, *38*, 1034 – 1054

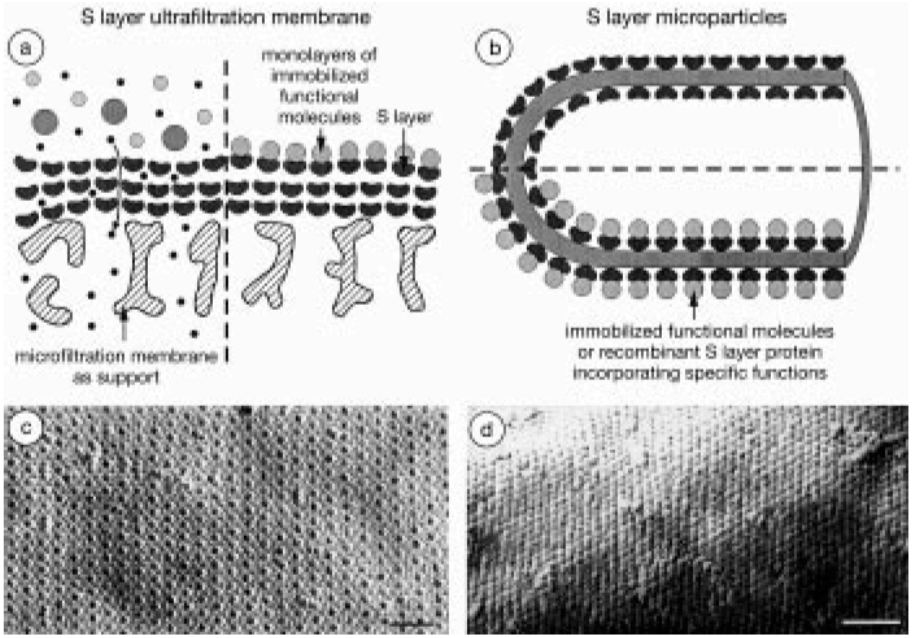

Figure 9. Schematic drawing showing a) S layer ultrafiltration membranes (SUMs) and b) S layer microparticles (SMPs) as matrix for the immobilization of functional macromolecules. c, d) Electron micrographs of freeze-etched preparations of S layers with hexagonal lattice symmetry. In (c) polycationic ferritin (PCF) was used for labeling negatively charged domains on the surface of the archaeon *Thermoproteus tenax*. In (d) ferritin was covalently linked to the carbodiimide-activated carboxy groups of the S layer lattice of *Thermoanaerobacter thermohydrosulfuricus*. The bars correspond to 100 nm.

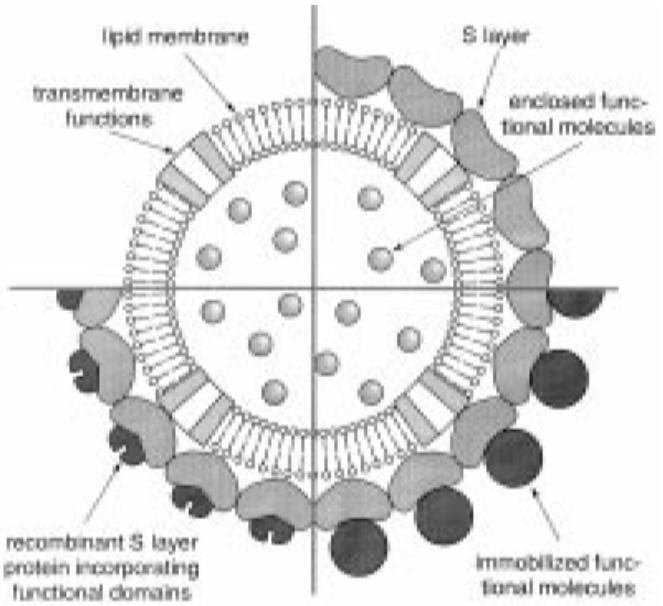

S-layer arrays

Angew. Chem. Int. Ed. **1999**, *38*, 1034 – 1054

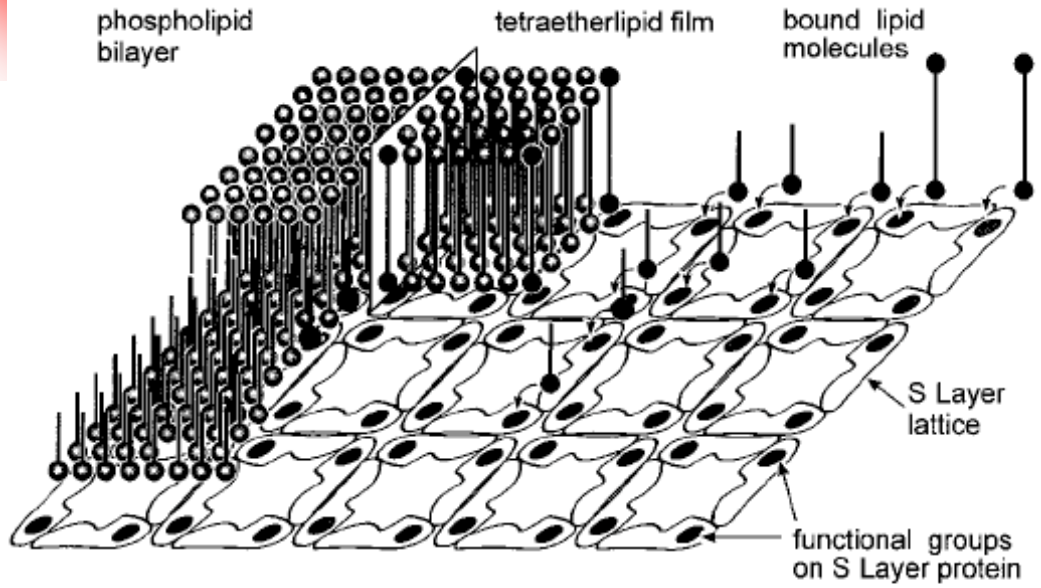

Figure 11. Schematic illustration of the "semifluid" membrane model composed of a phospholipid bilayer or tetraetherlipid monolayer Langmuir film supported by an S layer. The proportion of lipid molecules which can covalently be linked to the porous S layer lattice or which interact by noncovalent forces with domains of the S layer protein subunits significantly modulates the lateral diffusion of the free lipid molecules and consequently the fluidity of the membrane (modified based on reference [200]).

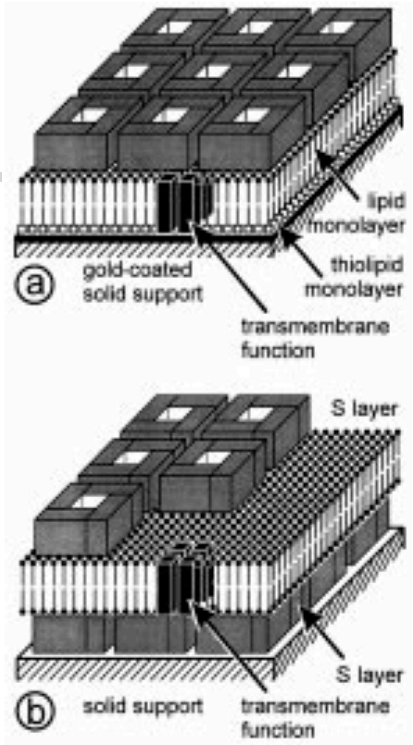

Figure 12. Schematic drawing illustrating the concept of solid-supported lipid membranes stabilized by S layers. In (a) the generation of the lipid bilayer makes use of the strong chemisorption of thiolipids to gold. The second leaflet and the S layer which had recrystallized at the lipid film before in a Langmuir trough were transferred onto the thiolipid-coated solid support by the Langmuir – Schaefer technique. Integrated functional molecules allow the investigation of transmembrane functions. b) As an alternative to soft polymer cushions an S layer is located between the solid support and the lipid layer. Optionally, the external leaflet of the lipid bilayer can be stabilized by the attachment of an S layer (modified based on

S-layer arrays

Angew. Chem. Int. Ed. **1999**, *38*, 1034 – 1054

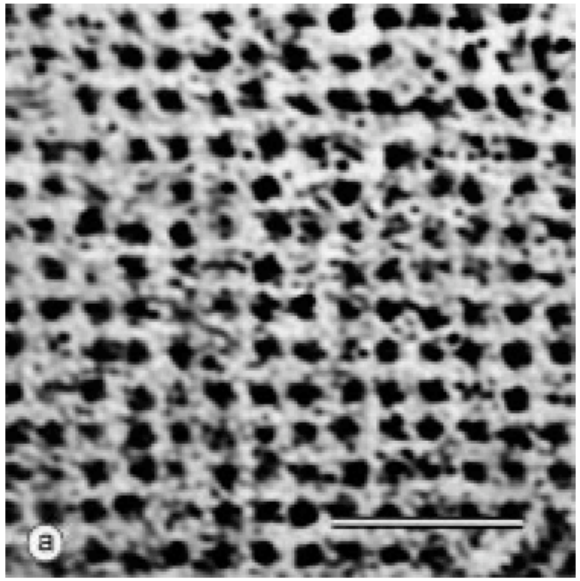

Figure 15. a) Electron micrograph of a gold "superlattice" consisting of monodisperse gold nanoparticles with mean diameters of 4 to 5 nm. b) Schematic drawing of a cross-section through a support coated with S layers, where the gold nanoparticles had formed in the pore region of the protein layer. The bar corresponds to 50 nm.

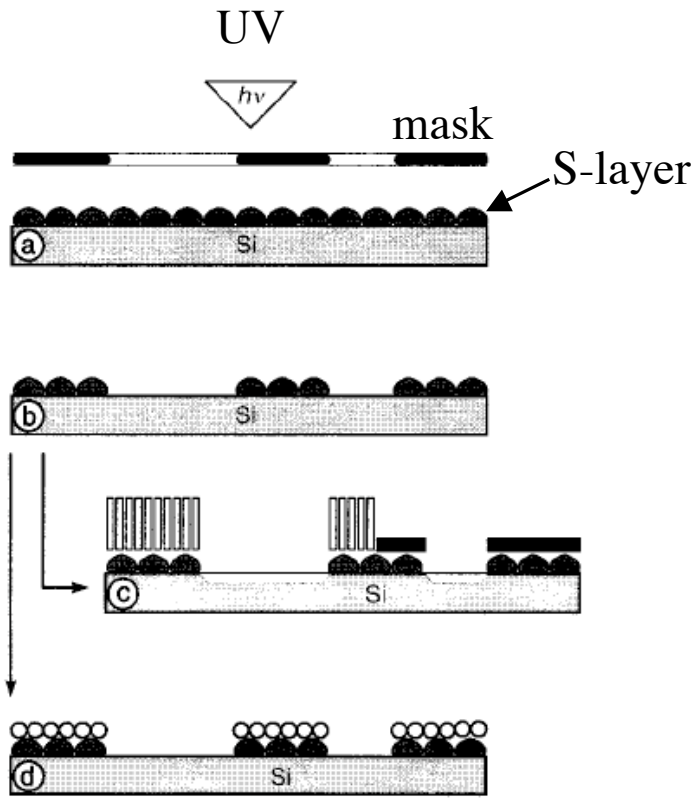

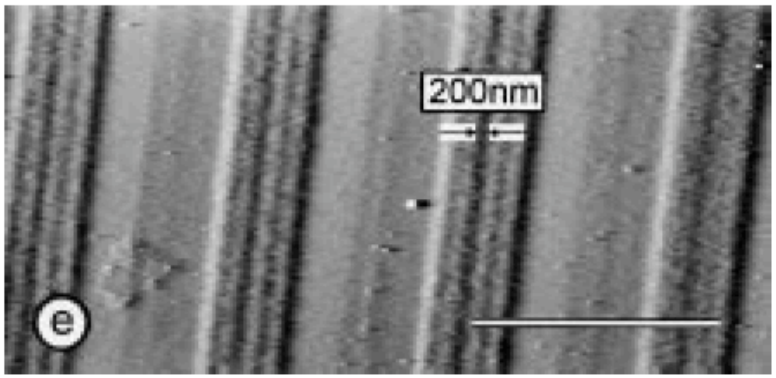

Bionanotech - proteins

- Engineering
- Design
- Catalysis
- Self-assemblies
- Templates & scaffolds
- Surface coatings
- Sensors

Self-assembling peptide templates

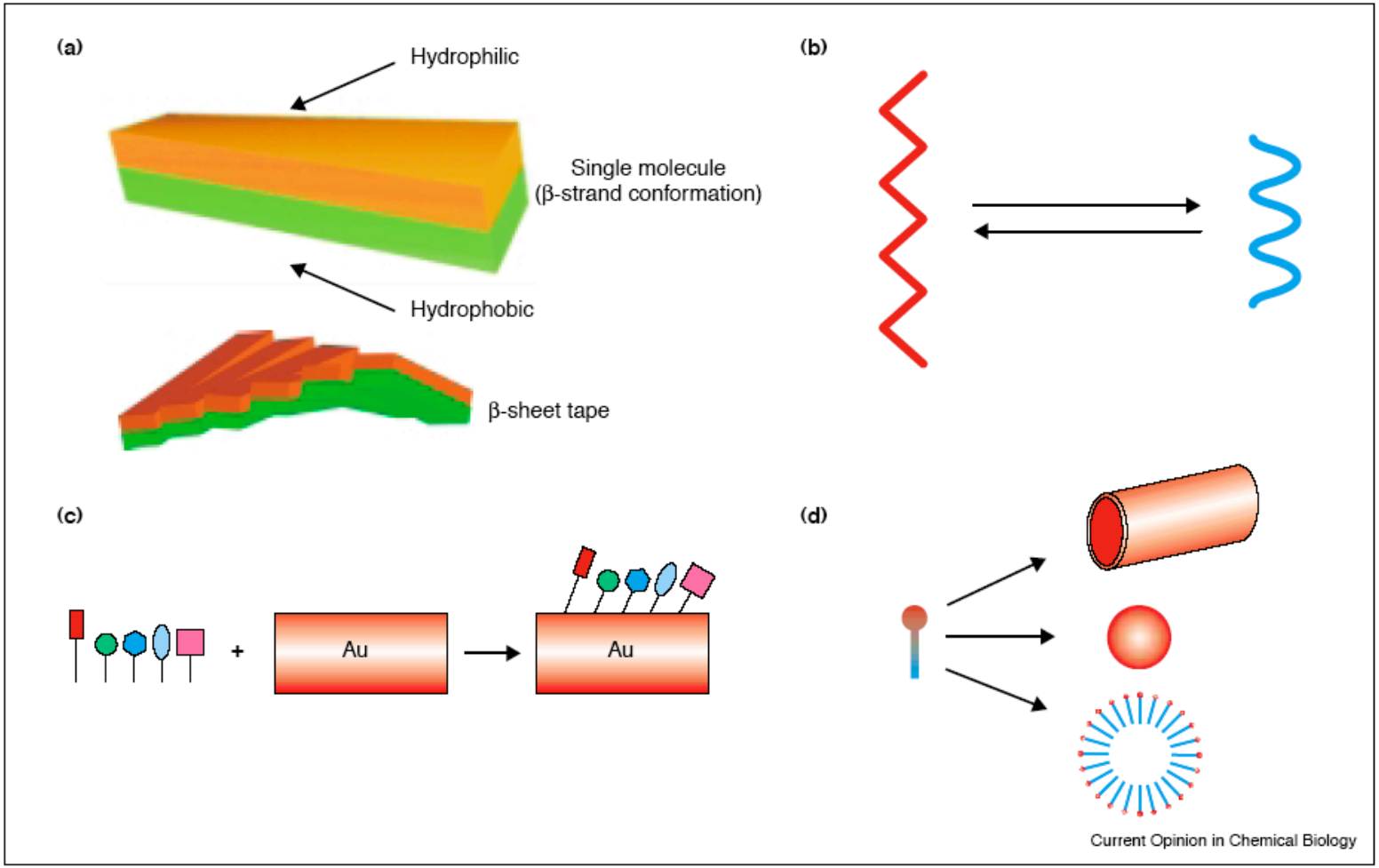

Various types of self-assembling peptide systems. **(a)** Amphiphilic peptides in β-strand conformation are chiral objects. As a consequence, they self-assemble into twisted tapes. **(b)** Helical dipolar peptides can undergo a conformational change between α-helix and β-sheet, much like a molecular switch [44•]. **(c)** Surface-binding peptides can form monolayers covalently bound to a surface [45•]. **(d)** Surfactant-like peptides can form vesicles and nanotubes [9••,10•].

Current Opinion in Chemical Biology 2002, 6:865–871

Self-assembling peptide templates

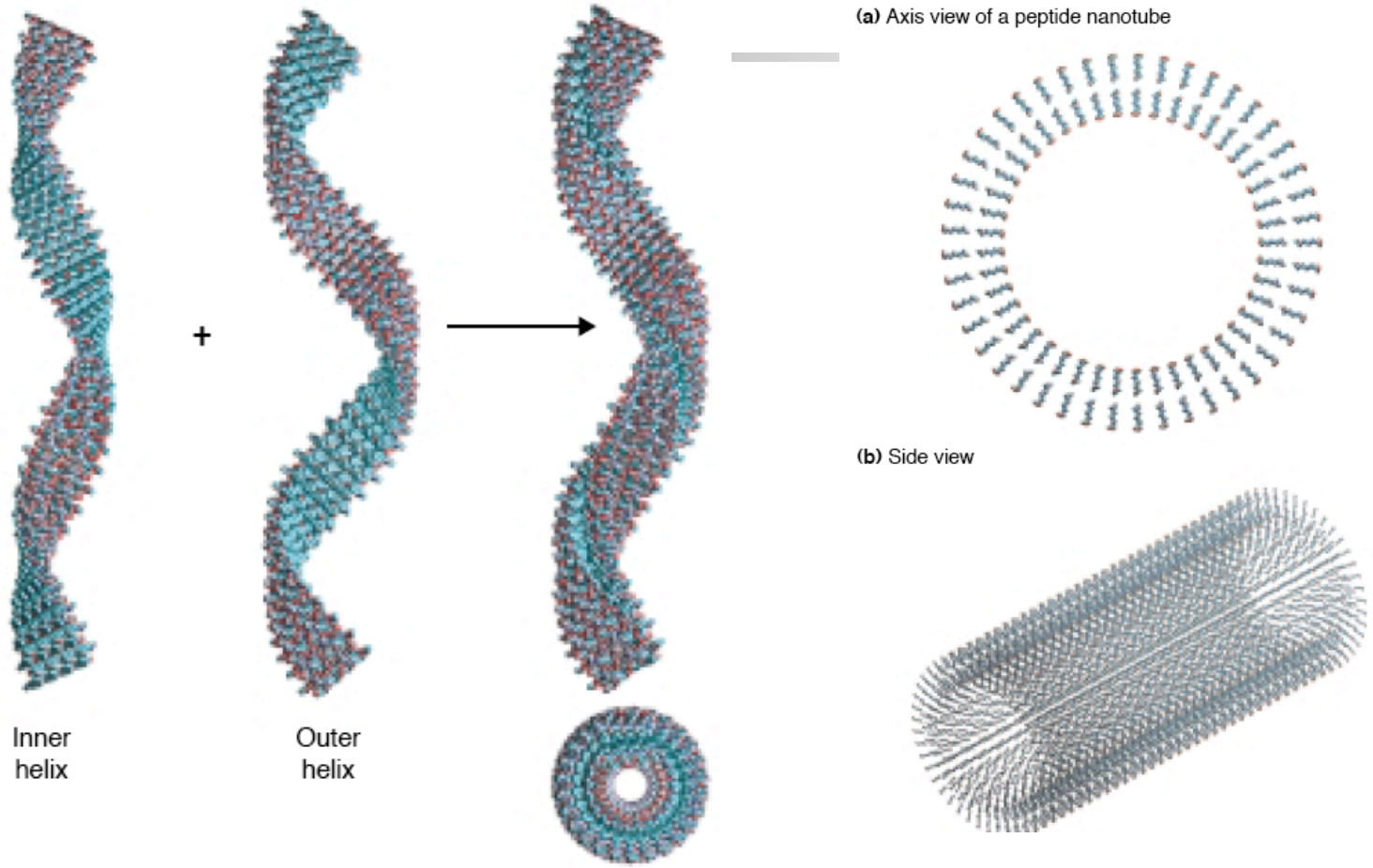

Current Opinion in Chemical Biology 2002, 6:865–871

Casting Metal Nanowires Within Discrete Self-Assembled Peptide Nanotubes

SCIENCE VOL 300 25 APRIL 2003

Meital Reches and Ehud Gazit*

Tubular nanostructures are suggested to have a wide range of applications in nanotechnology. We report our observation of the self-assembly of a very short peptide, the Alzheimer's β-amyloid diphenylalanine structural motif, into discrete and stiff nanotubes. Reduction of ionic silver within the nanotubes, followed by enzymatic degradation of the peptide backbone, resulted in the production of discrete nanowires with a long persistence length. The same dipeptide building block, made of D-phenylalanine, resulted in the production of enzymatically stable nanotubes.

Metal nanowires from peptide templates

SCIENCE VOL 300 25 APRIL 2003

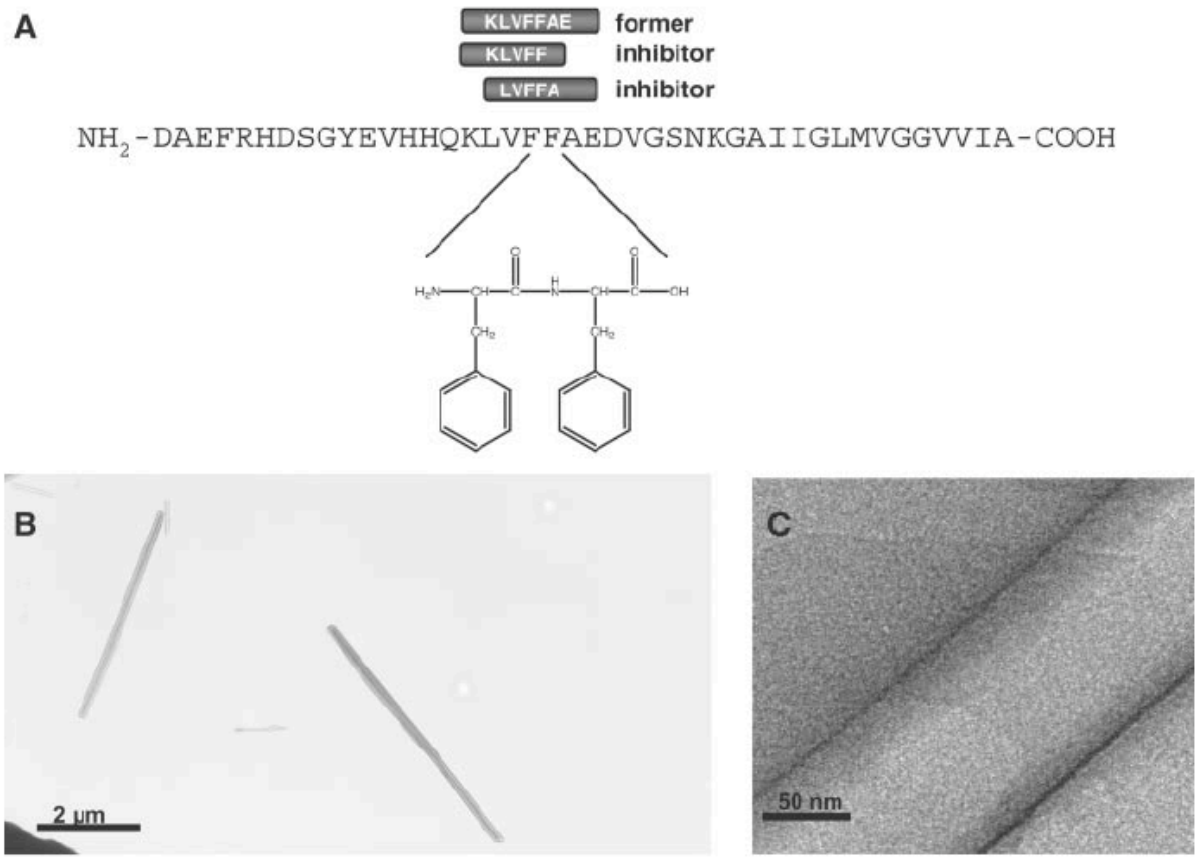

Fig. 1. Self-assembly of well-ordered and elongated peptide nanotubes by a molecular recognition motif derived from the β-amyloid polypeptide. (**A**) The central aromatic core of the β-amyloid polypeptide is involved in the molecular recognition process that leads to the formation of amyloid fibrils. Various fragments of the core form amyloid fibrils or inhibit their formation. (**B**) TEM images of the negatively stained nanotubes formed by the diphenylalanine peptide. (**C**) HR-TEM images of negatively stained peptide nanotubes, visualized by field emission gun microscope.

Metal nanowires from peptide templates

SCIENCE VOL 300 25 APRIL 2003

Fig. 2. Structural analysis of the tubular nanoparticles. (A) Low-magnification SEM images of a field of discrete nanotubes that are present as individual entities. (B) High-magnification SEM image of an individual nanotube. (C) A statistical distribution of nanotube diameters.

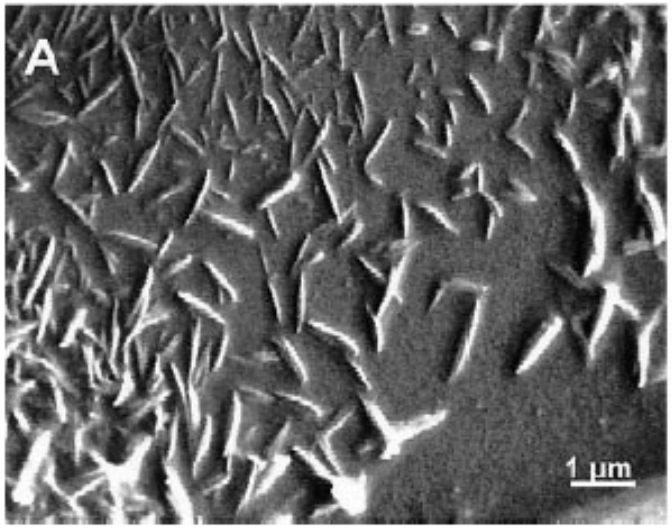

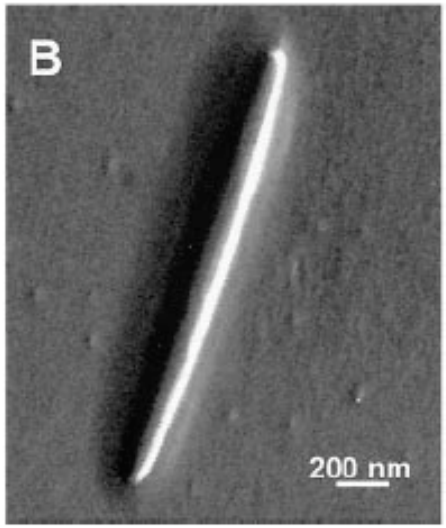

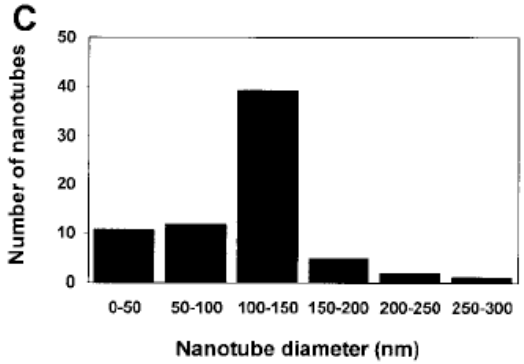

Metal nanowires from peptide templates

SCIENCE VOL 300 25 APRIL 2003

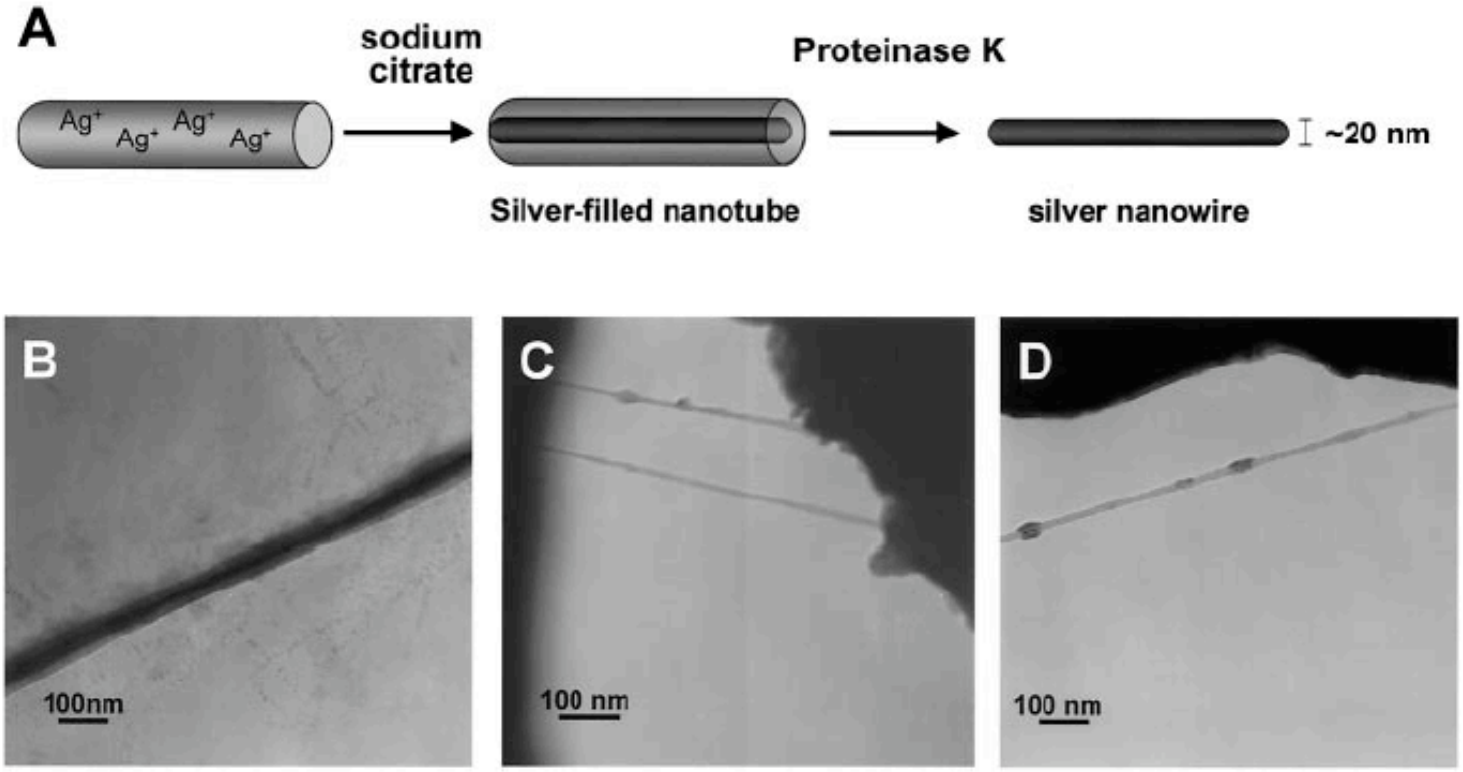

Fig. 3. Casting of silver nanowires with the peptide nanotubes. (**A**) The nanowires were formed by the reduction of silver ions within the tubes, followed by enzymatic degradation of the peptide mold. (**B**) TEM analysis (without staining) of peptide tubes filled with silver nanowires. (**C** and **D**) TEM images of silver nanowires that were obtained after the addition of the proteinase K enzyme to the nanotube solution.

Metal nanowires from peptide templates

SCIENCE VOL 300 25 APRIL 2003

Fig. 4. Formation of peptide nanotubes by different aromatic peptides. (A) TEM image of the stable nanotubes formed by the D–amino acid building-block analog (B) TEM image of a tubular structure formed by the NH_2-Phe-Trp-COOH dipeptide. Amorphous aggregates can be observed in the background.

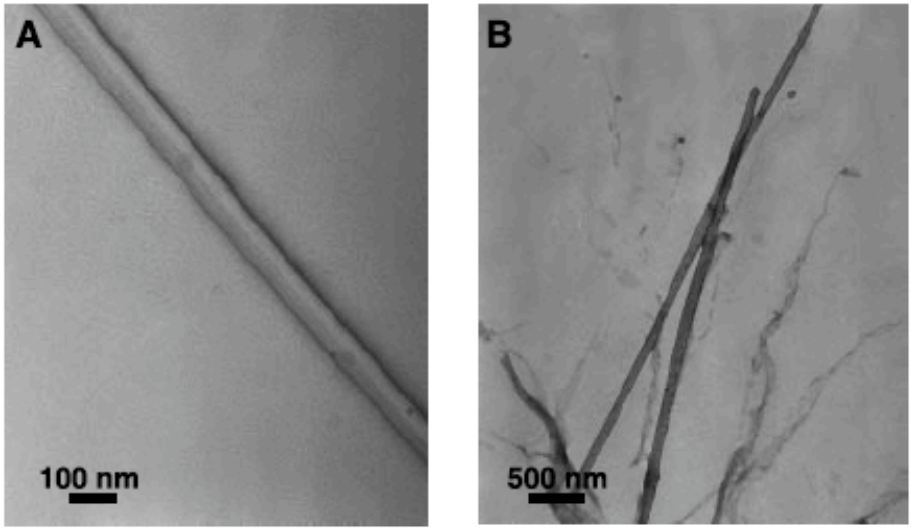

NH_2-D-Phe-D-Phe-D-COOH +Proteinase K

NH_2-L-Phe-L-Trp-COOH

Bionanotech - proteins

- Self-assemblies
- Templates & scaffolds
  - Nanoparticles
  - Metals
  - Silica, minerals, ceramics, semiconductor
- Surface coatings

Most Materials are "Biohostile"

AFFINERGY

Site-Specific Biological Delivery Systems

Daniel Kenan

www.affinergy.com

Interfacial Biomaterials (IFBM)

Objective:

Attach a specific **biological material** (cell, antibody, protein, etc.)

to...

A **synthetic material** (plastics, metals, glass, etc.)

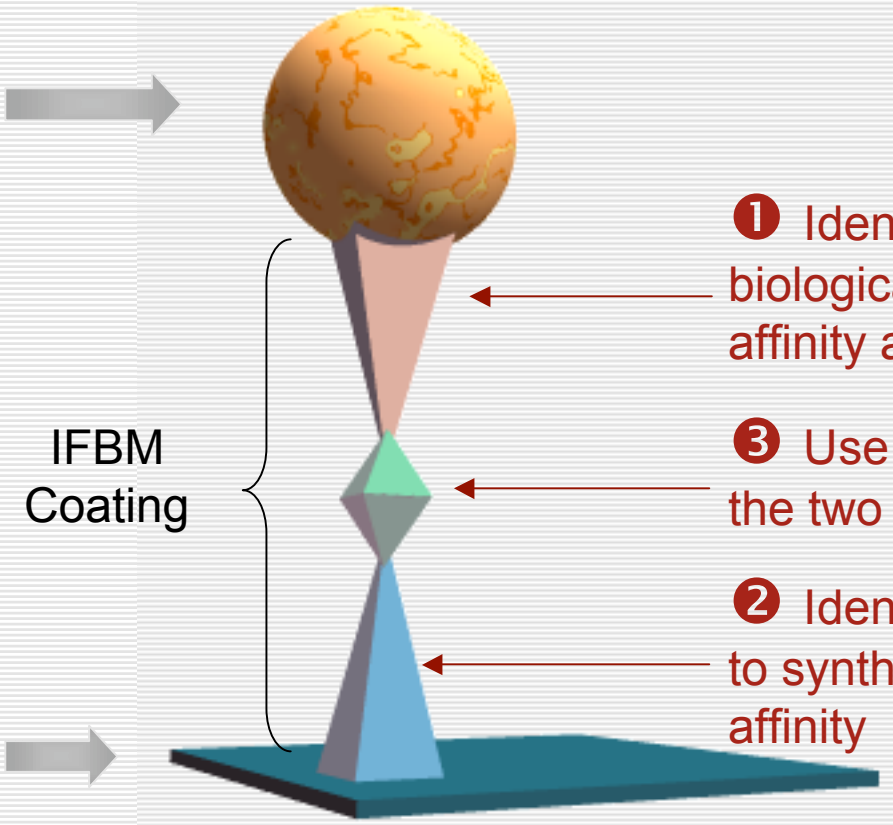

❶ Identify peptide that binds to biological material w/ high affinity and selectivity

❸ Use a small linker to tie the two peptides together

❷ Identify peptide that binds to synthetic material w/ high affinity

IFBMs Configured as Cell Attractants

Polystyrene Binding Peptide Synthesized with RGD

FFPSSWYSHLGVLSSGRGD

Titanium orthopedic screw with Stem Cells

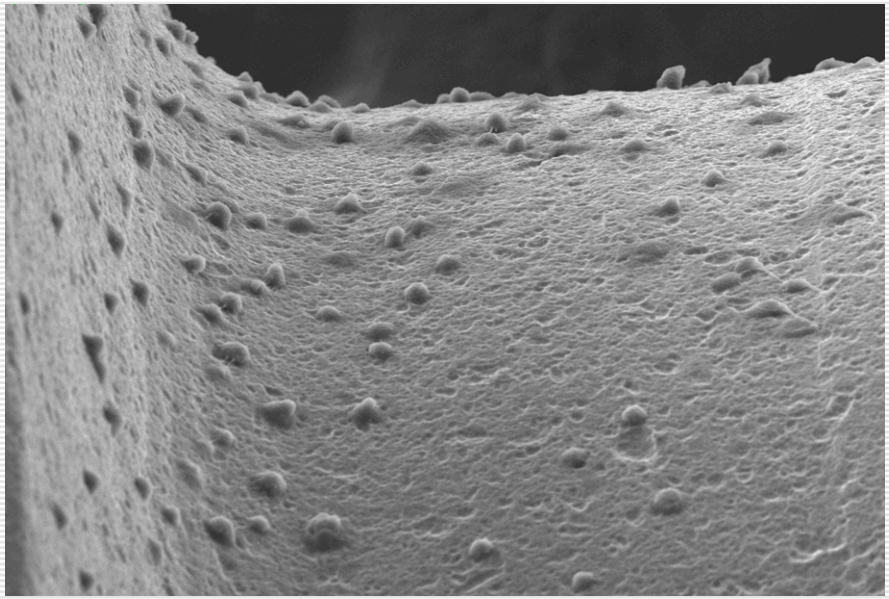

IFBM Attachment of preadipocytes

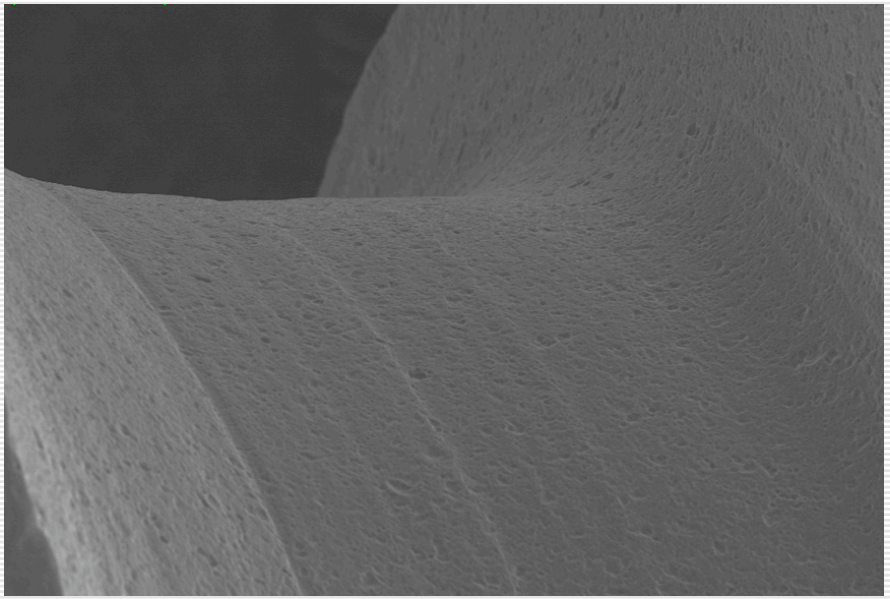

IFBM Blocking

AFFINERGY

IFBM's Mediate Rapid & Efficient Cell Adhesion on Ti

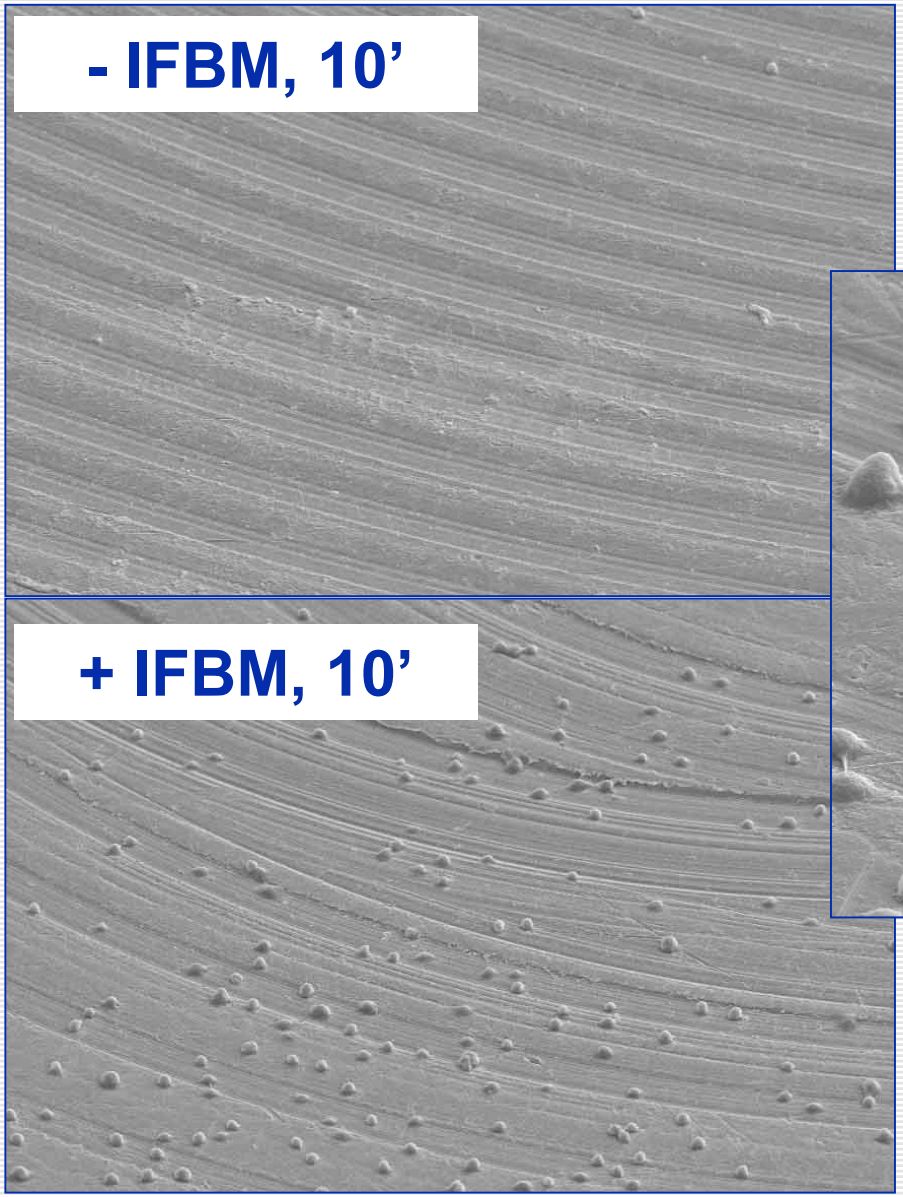

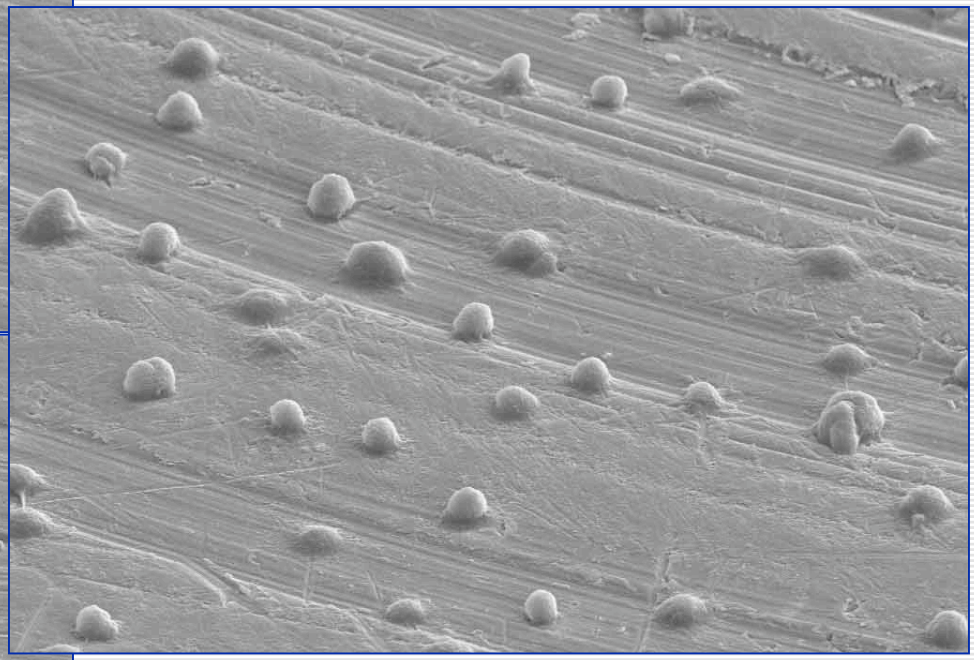

AFFINERGY

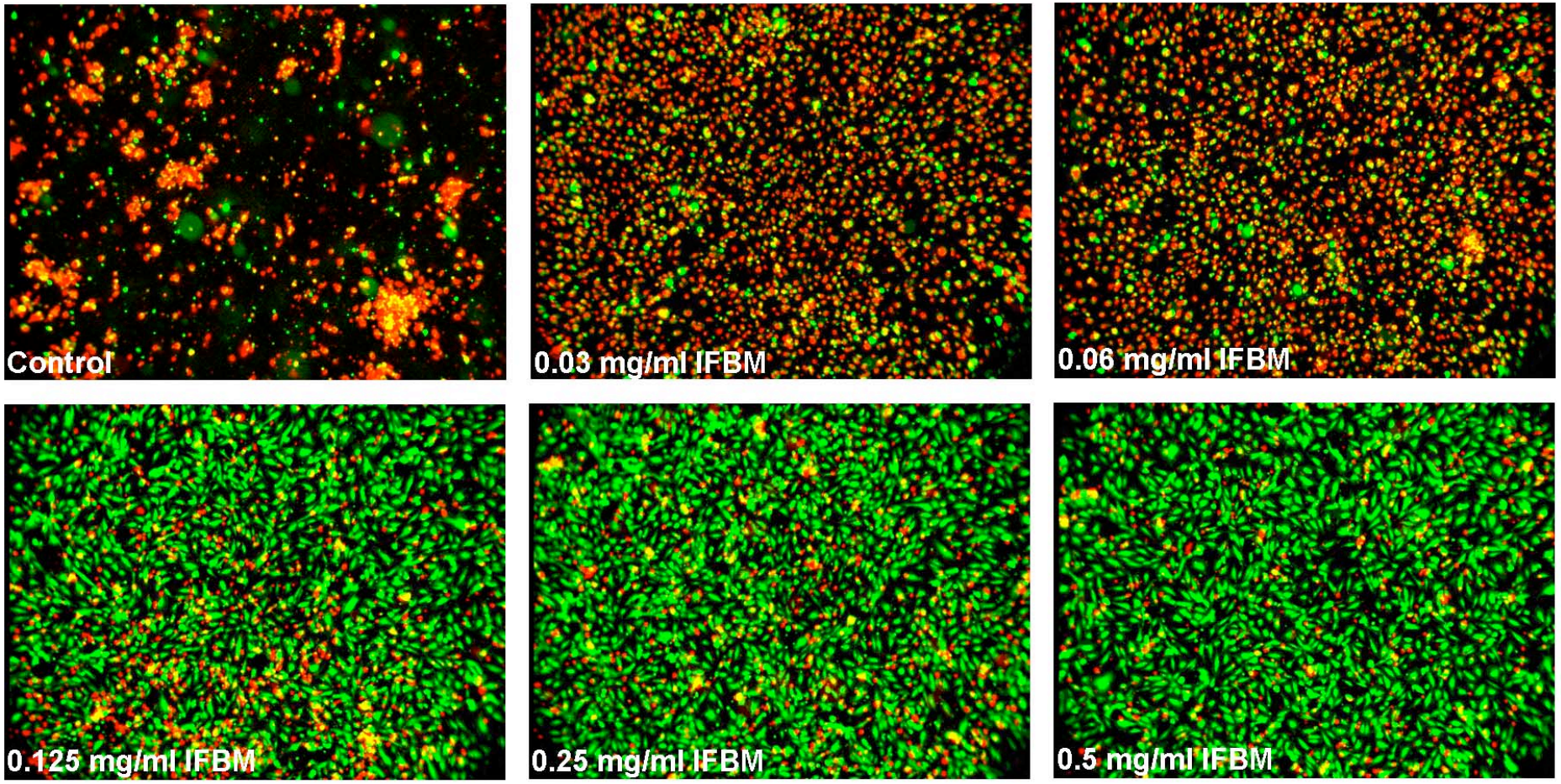
Control
0.03 mg/ml IFBM
0.06 mg/ml IFBM
0.125 mg/ml IFBM
0.25 mg/ml IFBM
0.5 mg/ml IFBM

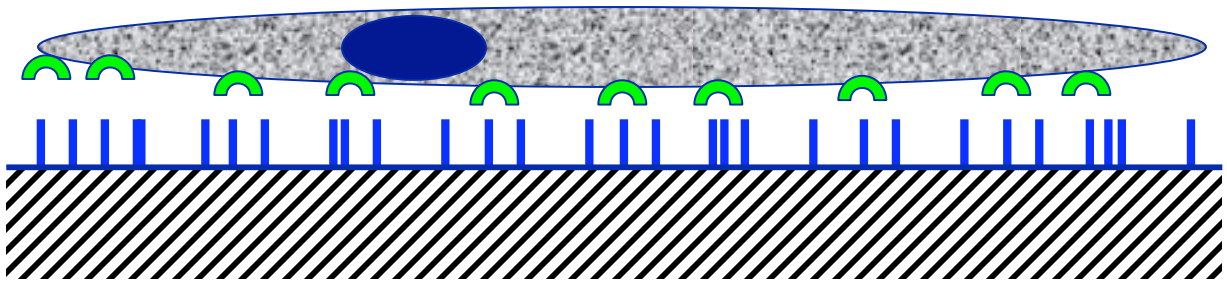

Mineralization of IFBM-Supported Stem Cells at 45d

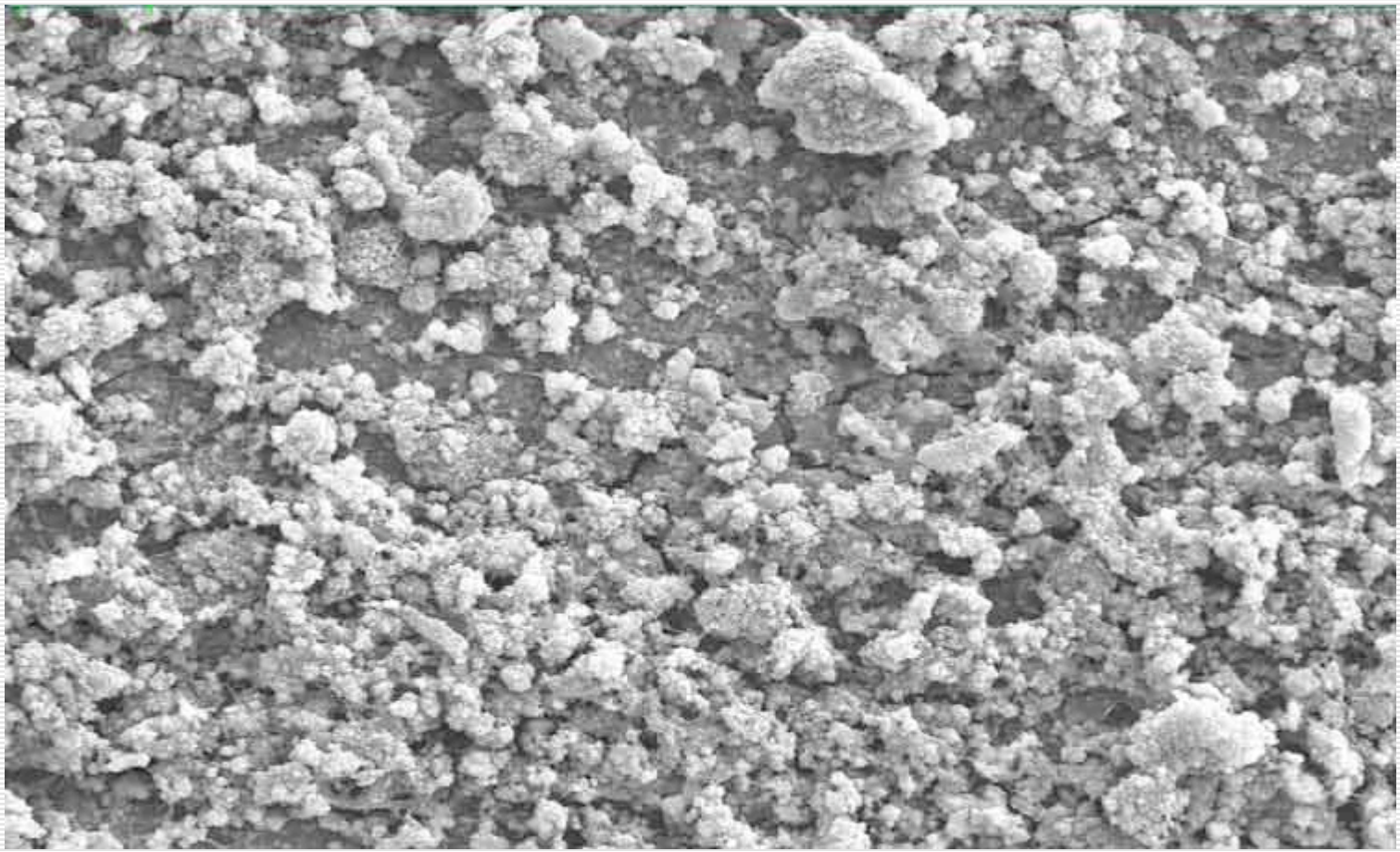

AFFINERGY

IFBM Platform

- Growth Factors
- Cell Receptors
- Cell Matrix Proteins
- Collagen
- Enzymes
- Antibodies

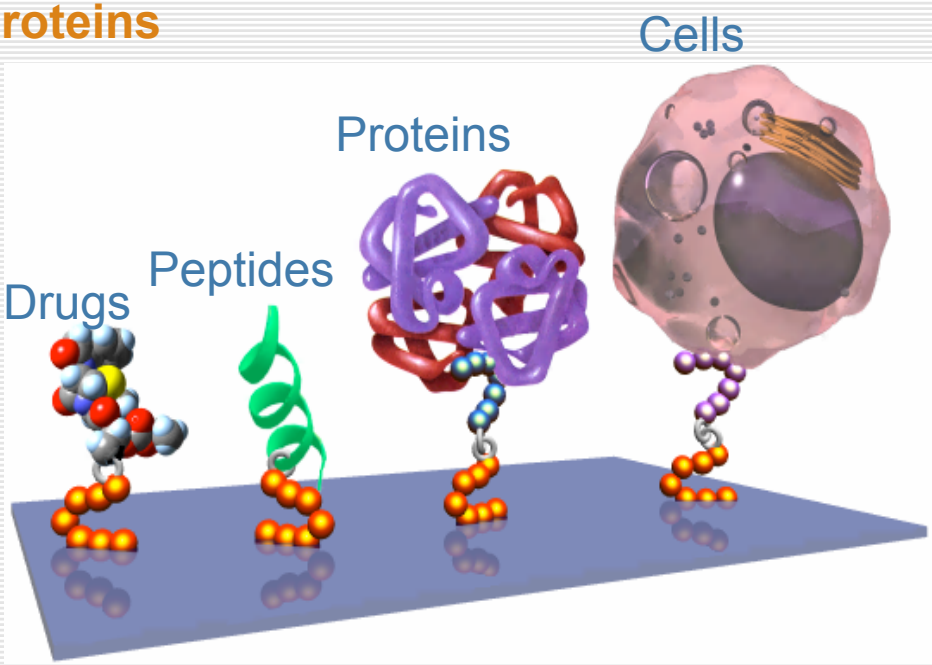

- Titanium
- Stainless Steel
- Teflon
- PET, PETG, PGA
- Polystyrene
- Polycarbonate
- Glass, Nylon, Latex

IFBM Discovery Platform:

> 4 billion peptides in libraries

3 to 6 month cycle to find binders

Binders found for every target tried

Biases can be built into selection

Range of affinities and specificities can be exploited

Rapid Solutions Due to Modularity of Affinergy's Platform

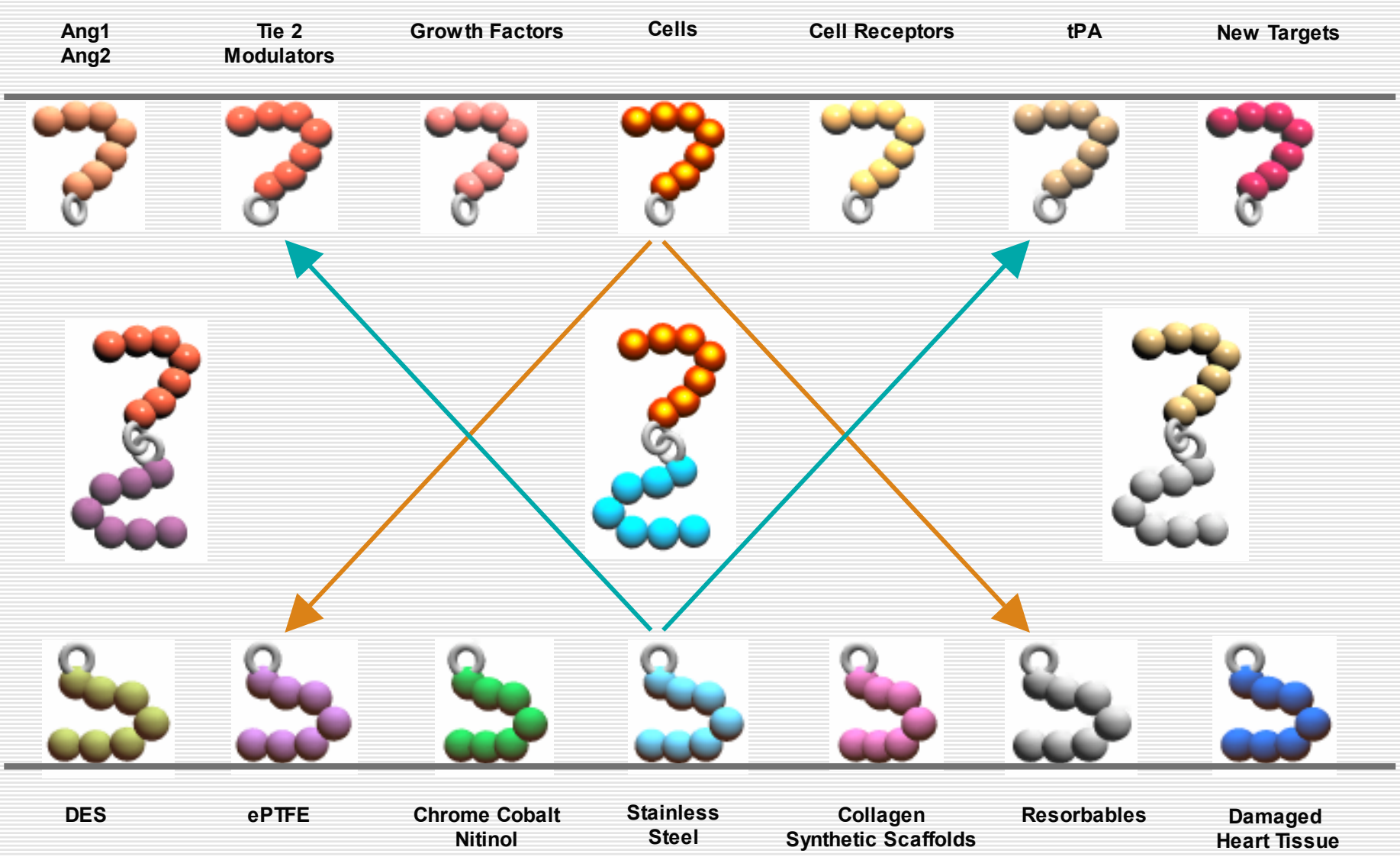

Bionanotech - proteins

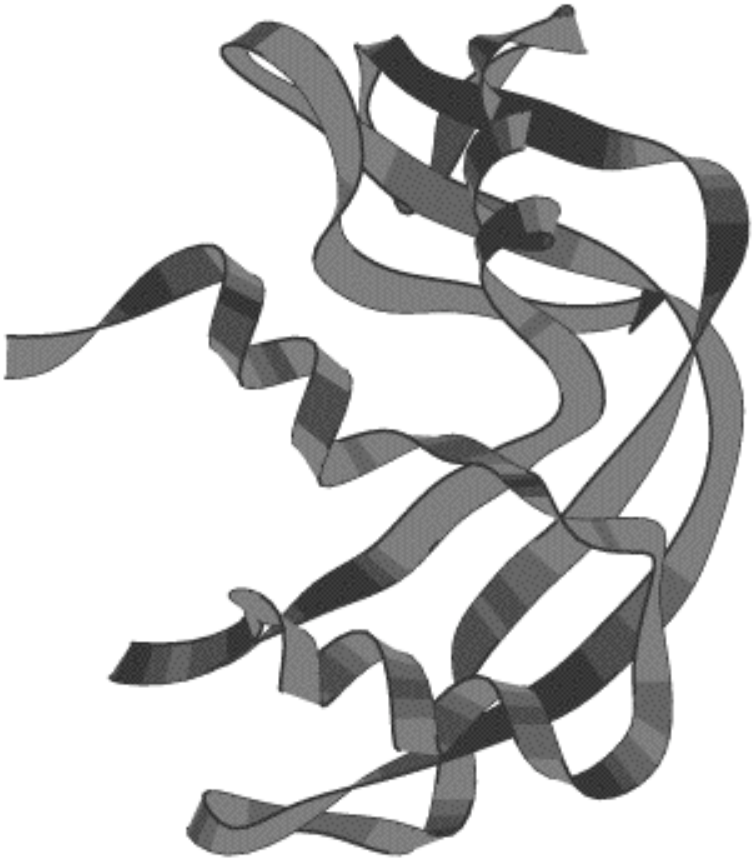

- Engineering & design
  - Custom catalysts
- Self-assemblies
  - Nano organizers
- Templates & scaffolds
- Surface coatings
  - Nanoimprint or DPN inks
  - Tissue regeneration
- Sensors
  - Sensitivity & selectivity

Molecularly Imprinted Polymers

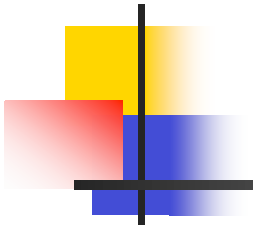

- “Artificial proteins”
- Mimic protein functions
  - Molecular recognition (binding)
  - Catalysis
- Higher stability
- Manufacture greater quantities

Molecularly Imprinted Polymers

Imprinted polymers—Tailor-made mimics of antibodies and receptors

CHEM. COMMUN., 2003, 171–178

Karsten Haupt†
University of Paris 12, Science Faculty, Créteil, France. E-mail: karsten.haupt@tbiokem.lth.se

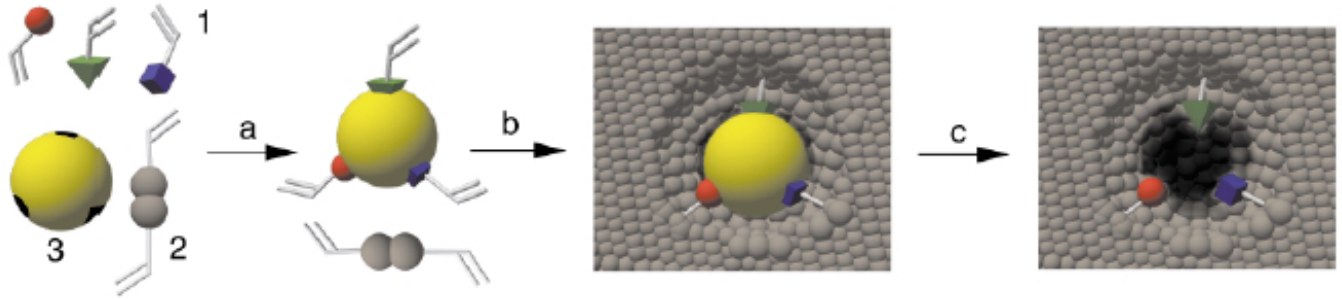

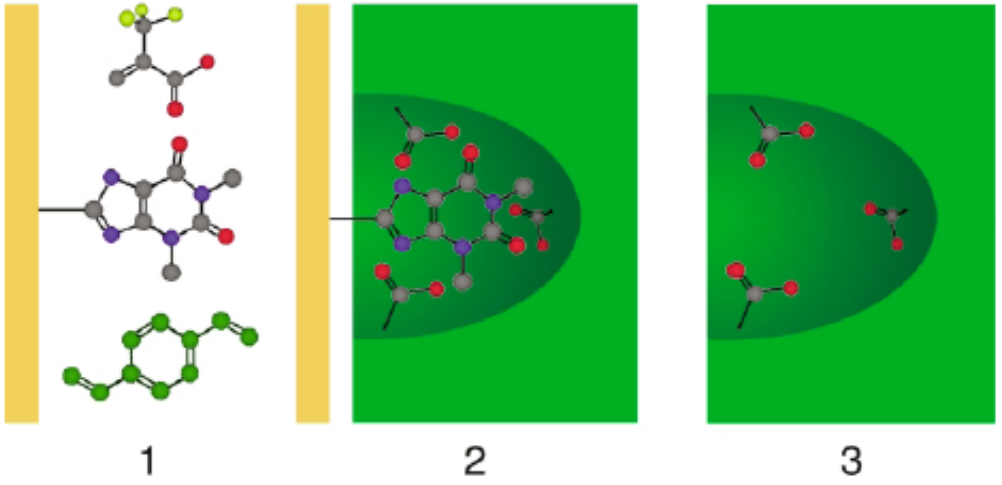

Fig. 3 Molecular imprinting of theophylline immobilized onto a solid support: immobilized template with monomers (1), composite material after polymerization (2), imprinted polymer after dissolution of the support (3).[26]

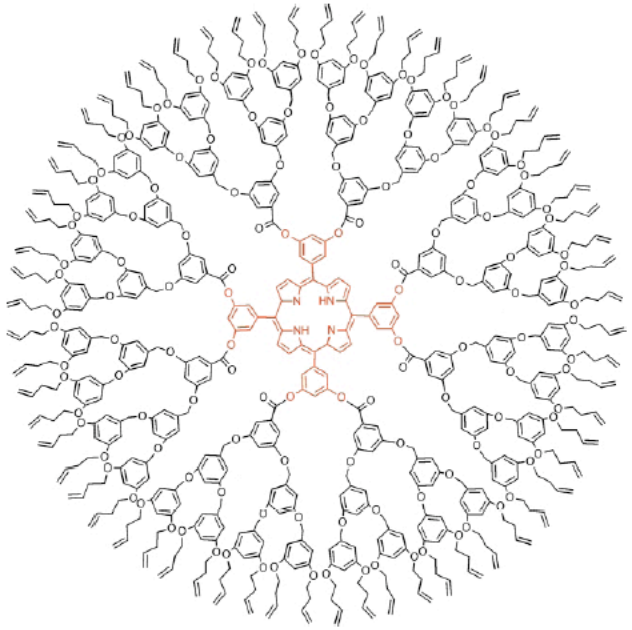

Fig. 2 A dendrimer with cross-linkable double bonds at the outer shell, and the covalently attached porphyrin template (in red) in the core.[24]

Molecularly Imprinted Polymers

CHEM. COMMUN., 2003, 171–178

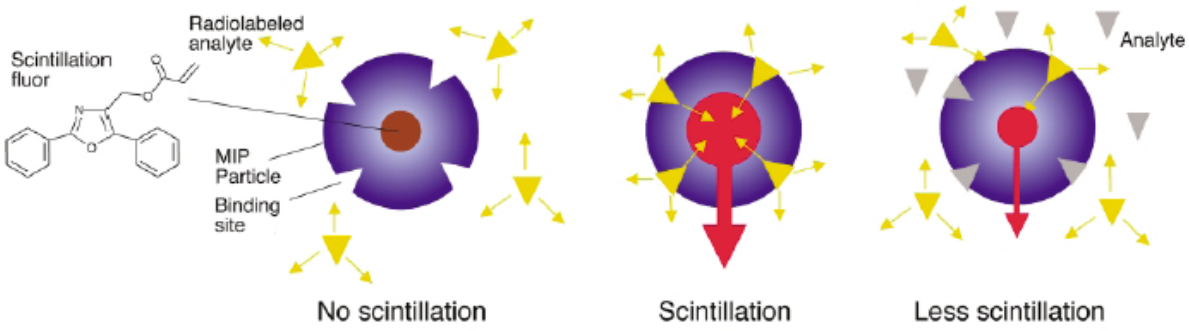

Fig. 6 Schematic representation of a competitive binding assay format based on proximity scintillation.[44]

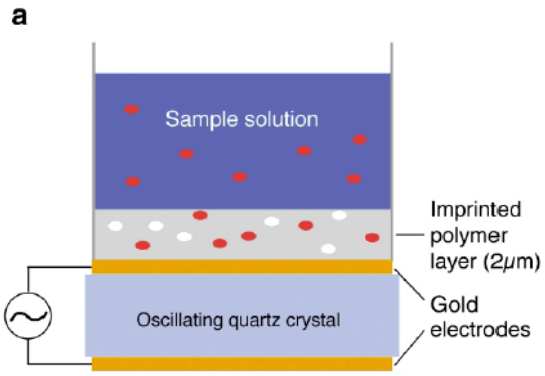

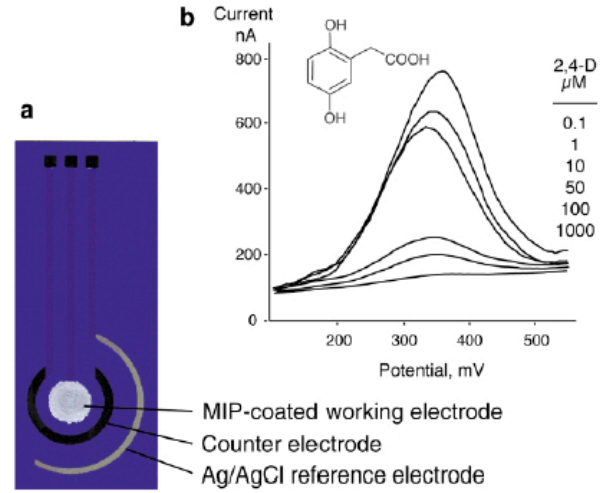

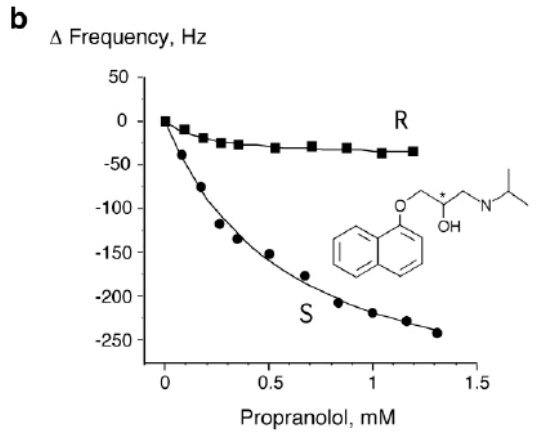

Fig. 8 (a) Screen-printed electrode coated with MIP-microparticles. The particles are covered with a thin agarose membrane. (b) Structure of the electroactive probe 2,5-dihydroxyphenylacetic acid, and differential pulse voltammetric scans obtained in the presence of different concentrations of the analyte 2,4-D.[38]